A MODIFIED SHAO-C TROPOSPHERIC DELAY CORRECTION MODEL FOR ETHIOPIA

A Thesis Submited in Partial Fulfillment of the
Requirments for the Degree of
Master of Science in Physics

Addis Ababa University
School of Graduate Studies

Yohannes Getachew
Addis Ababa, Ethiopia
June 2013

Addis Ababa University
School of Graduate Studies
College of Natural Sciences
Faculty of Chemical and Physical Sciences
Department of Physics

The undersigned here by certify that they have read and recommend to the School of Graduate Studies for acceptance a thesis entitled "**A MODIFIED SHAO-C TROPOSPHERIC DELAY CORRECTION MODEL FOR ETHIOPA**" by **Yohannes Getachew** in partial fulfillment of the requirements for the degree of **Master of Science in Physics**.

Dated: June 2013

Approved by the Examination Committee:

Dr. Gizaw Mengistu, Advisor

Prof. A.V. Gholap, Examiner

Dr. Kassahun Ture, Examiner

ADDIS ABABA UNIVERSITY

Date: **June 2013**

Author: **Yohannes Getachew**

Title: **A Modified SHAO-C Tropospheric Delay Correction Model For Ethiopia**

Department: **Department of Physics**

Degree: **M.Sc.** Convocation: **JUNE** Year: **2013**

Signature of Author

Table of Contents

List of Figures

Abstract

The troposphere affects electromagnetic signal propagation causing signal path bending and the alteration of the electromagnetic wave velocity. Tropospheric delay can introduce a considerable error in satellite positioning if it is not properly estimated. The average GPS signal delay in the zenith direction can vary from 1.8 m to 2.5 m depending on meteorological conditions and site location. In this work, the spatial and temporal variations of the zenith tropospheric delay (ZTD), zenith wet delay (ZWD) and precipitable water(PW) over Ethiopia, are analyzed using ECMWF (European Centre for Medium-Range Weather Forecast) ERA-interim pressure-level atmospheric data and compared with ZTD time series for 5-year period from 2007-2011 measured at several GPS stations from the Crustal Movement Observation Network of over Great Rift Valley regions of Eastern Africa which are managed by UNAVCO (University NAVstar COnsortium). A modified version of tropospheric delay correction model, SHAO-C used in China, is assessed for its performance over Ethiopia. ZTD is modeled directly by a cosine function together with an initial value and an amplitude at a reference height in each grid, and the variation of ZTD along altitude, latitude and longitude is fitted with a second order polynomials. The coefficients of the modified SHAO-C are generated using the ECMWF ERA-Interim data at 0.75x0.75 degree latitude-longitude grid, featuring regional characteristics in order to facilitate a wide range of navigation and other surveying applications. The altitude is obtained from high resolution Digital Elevation Model (DEM). The overall average bias ranges between -4.3 cm to -1 cm for ZTD, -3.42 cm to -0.584 cm for ZWD and -1.12 cm to -0.34 cm for PW, and the RMSE is less than 4.5 cm. The results are assessed for fulfilling the requirements of most GNSS navigation or positioning applications in terms of the tropospheric delay correction.

Acknowledgements

Firstly I would like to express my sincere thanks to my advisor and instructor Dr. Gizaw Mengsiitu for his critical comments, assistance, supervision and strong guidance while I am working on this thesis. Secondly I would like to thank Dr. Addisu Hunegnaw for his support and contineously gudance me on GAMIT software, all geodesy Department members for providing the laboratory room and computers. I would like to express my heart feling and gratitude to all friends for providing encouragement and support.
Thirdly I would like to acknowledge SHAO-C correction model developers Dr. SONG ShuLi1 and Chinas Science academy .

Finally the numerical weather model data were freely down loaded from ECMWF, and the GPS data were freely accessed from UNAVCO, CDDIS and SOPAC. I would like to acknowledge ECMWF, UNAVCO, CDDIS and SOPAC.

Acronyms

CDDIS	Crustal Dynamics Data Information System
DGPS	Differential GPS
ECMWF	European Center for Medium-Range Weather Forecasts
GAMIT	GPS at MIT
GNSS	Global Navigation Satellite System
GPS	Global Positioning System
DEM	Digital Elevation Model
C/A	Coarse acquisition
IGS	International GPS Service
RF	Radio Frequency
RMSE	Root mean square Error
NWM	Numerical weather model
NWP	Numerical weather prediction
PW	Precipitable water
SOPAC	Scripps Orbit and Permanent Array Center
TEC	Total Electron Content
UNAVCO	University NAVstar COnsortium
ZTD	The tropospheric zenith total delay
ZHD	Zenith Hydrostatic Delay
ZWD	The tropospheric zenith wet delay

Chapter 1

Introduction

The influence of atmosphere, in the form of delay on the propagation of electromagnetic microwaves signals emitted from the Global Positioning System (GPS), is one of the main accuracy limiting factor of positions determined by GPS. It is a serious error in GPS measurements both through ray path bending and the modification of the electromagnetic velocity.

Based on electromagnetic wave interaction the atmosphere is divided into two, ionosphere and neutral atmosphere. Ionosphere is an electrically charged region of the earth's atmosphere, which starts from ∼50 km extends upto 1000 km above the surface of the earth. The GPS signal delay occurrs due to total electron content (TEC) present in the ionosphere[1]. While the neutral atmosphere is the non electrically charged region of the earth's atmosphere, which extends from the earths surface up to an altitude of approximately 50km (includes the troposphere and stratosphere), the effect is termed as tropospheric delay, because most of the mass of neutral atmosphere is in the troposphere. The tropospheric total delay can be split into two: hydrostatic delay (Dry delay), ZHD, and non-Hydrostatic delay (Wet delay), ZWD. The hydrostatic delay, ZHD, is caused by dry air, which accounts for about 90 percent of the total delay and typically around 2.3 m at the zenith[2]. While the non hydrostatic delay (wet zenith delay) is due to temporal and spatial variability of water vapor, its non-hydrostatic counterpart is normally around less than ∼0.4 m [3]. The tropospheric wet delay and water vapor are interdependent with each other. Precipitable water vapor (PWV) is one of the most environmental parameters that play a key role of the Earths atmosphere.

Recently, many neutral atmospheric delay model, such as UNB3m (University of New Brunswick modified version) neutral atmospheric model, SHAO-C tropospheric model were developed. The UNB3m neutral atmospheric model is a global model, which uses

the Saastamoinen zenith delays with annual mean and amplitude for the temperature, pressure, water vapor pressure, temperature lapse rate and water vapor pressure decline rate are provided on the mean sea level. However, the SHAO-C tropospheric correction model is a regional model over China's area, which uses a numerical weather model called ECMWF with the over all bias and RMSE of 2.0 and 4.5 cm, respectively[4]. It is better and sufficient for most GNSS navigation or positioning applications in terms of the tropospheric delay correction over the region compared to UNB3m.

In the recent past, a regional zenith troposphere delay model (neutral atmospheric delay model) is not done over Ethiopia as well as in East Africa, but atmospheric precipitable water from ground-based GPS measurements and ERA-Interim Reanalysis were analyzed by Mengistu[6]. In this work, the feasibility and accuracy of the ECMWF data are assessed for use in tropospheric delay correction. The ZTD correction model in Ethiopia and its neighbors based on SHAO-C tropospheric correction model is intended for navigation and positioning users with high accuracy requirements. The time resolution of the data is 6 h, namely at 0, 6, 12, 18 UTC. The ERA-Interim pressure level meteorological data include temperature, specific humidity and geopotential height. Further, we derived precipitable water vapor by using zenith wet delay from the model , and the validation over the region was good agreement with GPS measurement value.

The thesis is organized as follows. Chapter 2 presents the general overview and introduction of GPS system. GPS observables are described and different errors affecting GPS observations are discussed. These covers ephemeris errors, satellite clock errors, receiver errors, multi path errors and errors due to atmospheric effects (the ionospheric and tropospheric range delays), are introduced. Chapter 3 provides description of the GPS processing software is known as GAMIT/GLOBK. It includes the general over view, data acquisition system and data preparation for the GAMIT software. This chapter also presents how to estimate and extracte estimates of a zenith delay and precipitable water using GAMIT. Chapter 4 presents the structure and physics of the troposphere, the tropospheric effect on GPS signal when electromagnetic wave propagates in the neutral atmosphere with the refractive index, and the revision of some significant number of troposphere delay models that reported in the scientific literature in the last few decades. Chapter 5 describes the algorithm and methodology of data extraction system from ECMWF ERA-Interim for use in SHAO-C tropospheric delay model over Ethiopia and its neighbors. The tropospheric path delay is defined in terms of refractive index mathematically and fitted harmonically with its dependency of spatial and temporal variations for the GPS signals (electromagnetic

wave signals). The model function parameters (coefficients) are defined and established, in addition the precipitable water vapor (PWV) is also defined in terms of zenith wet delay and mean temperature. Chapter 6 gives results and discussion. The tropospheric zenith total delay characteristics are analyzed using GPS measurements from different GPS stations over Ethiopia and its surrounding. The model parameters are assessed and mapped over the region. The model zenith total delay, wet delay and the derived precipitable water validation is also discussed by comparing with the GPS measurement. Finally Chapter 7 gives conclusions.

1.1 Objective

The main objectives of this thesis is :

1. To develop and test a tropospheric propagation delay model over Ethiopia, for featuring regional characteristics

2. To analyze the accuracy and adaptability of a regional GPS zenith troposphere error correction models over Ethiopia in order to facilitate a wide range of navigation and positioning applications in and around Ethiopia.

1.2 Scope and limitation

Due to time constraints and lack of continuous GPS observations, the following bounds are defined:

1. For the whole days of each year of data from Ethiopian GPS receiver stations center of the years 2007, 2008, 2009, 2010, and 2011 are processed. Data is chosen in the same period of the year to minimize the unknown impact of seasonality on the GPS results, thus reducing aliasing problems in the incipient time series.

2. Only GPS zenith delay and Precipitable Water were used for validation of the model precision and compression purpose.

3. Lack of real-time continuous meteorological data to quantify the state of the atmosphere

Chapter 2

Global Positioning System

2.1 Overview of GPS System

The Global Positioning System (GPS) is a satellite-based navigation system for accurate and instantaneous position determination and timing. The primary objective of GPS was to meet the needs of the US military and national security, in regards to positioning and timing, on a 24 hour per day basis all around the world and under all weather conditions [7]. The present constellation (up to January, 2013) consists of nominally 32 satellites and provides global coverage with four to eight satellites simultaneously observed above 15^o elevation. GPS has also become the primary radio positioning navigation system for civilian users in many aspects of everyday life. It is used for navigation in cellular telephones, cars, boats, and airplanes, for precise positioning in surveying, monitoring structures and the crust of the Earth, and for transferring precise time for banking transactions and a myriad of other scientific applications.

The two currently available global navigation satellite systems (GNSS) are the Russian Federation Global Navigation Satellite System (GLONASS) and the United States system, NAVSTAR (Navigation System with Timing and Ranging) Global Positioning System (GPS) [7].

The US NAVSTAR Global Positioning System (GPS) [7] was first conceived when the US Department of Defense approved its basic architecture in 1973. The system was declared fully operational in 1995 [7] and since that time, only minor improvements and maintenance have kept the system in excellent reliable working condition.

GPS navigation and position determination is based on measuring the distance from the user to known locations of the GPS satellites as they orbit. It is possible to determine three

coordinates of users positions (latitude, longitude, and altitude) as well as GPS receiver clock time offset using range measurements to four satellites. This increased accuracy allows the distance between the GPS receiver and GPS satellites to be determined with centimeter accuracy such that it is possible to estimate the atmospheric delay from GPS measurements.

GPS technology requires the following three segments:

- space segment,
- control segment and
- user segment.

2.1.1 Space Segment

GPS satellite travel at approximately 7,000 miles per hour about 12,000 miles (20,200 km) above the earths surface. The orbital planes are inclined 55.6^o with respect to the equator[8].

The GPS satellites provide a platform for radio transmitters, computers, and various

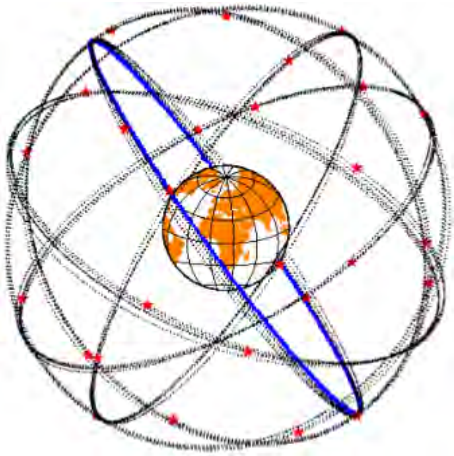

Figure 2.1: The orbital configuration of GPS Stellites (thaken from *http* : $//www.google.com/images?q = GPS + constellation\&channel$)

equipment used for positioning, timing, RF transmission and for a series of other military projects. The satellites are equipped with solar panels for power supply, reaction wheels for altitude control, and a propulsion system for orbit adjustments. The satellites transmit at frequencies L1 at $1575.42MHz$ and $L2$ at $1227.60MHz$ modulated with two types of codes and the navigation message. The codes are Precise Code (P-Code) and the Coarse

Acquisition Code (C/A Code). The P-Code generated at the fundamental frequency (i.e. 10.23 MHz) is available on both L1 and L2. The C/A Code modulated on only the L1 frequency. The navigation message is generated at a low frequency of $50Hz$ and is modulated on both L1 and L2 carrier frequencies[7]. It contains information on the ephemerids of the satellites, GPS time, clock behaviour, and system status messages.

2.1.2 The Control Segment

The operational control systems contains a master control station, monitor stations, and ground control stations. The master control station is located at Schriever Air Force Base in Colorado Springs[7]. It collects the tracking data from five monitor stations and calculates the satellite orbit and clock parameters. These results are then passed to one of the three ground stations for eventual upload to the satellites. The five monitor stations are equipped with precise cesium time standards and receivers that continuously measure range data to determine the broadcast ephemerids as well as model the satellite clocks. The ground stations mainly consist of ground antennas that receive the satellite ephemerids and clock information and upload them to each GPS satellite. In general the specific function of the control segment are to monitor the satellite orbit, to maintain GPS time, to predict satellite ephemerids and clock parameters, to update satellite navigation massages[7].

2.1.3 User Segment

The user segment consists of receiver technologies for computing local position/navigation solutions, in addition to the receiver clock offset. The GPS satellite positions are computed in the Earth centered Earth-fixed WGS-84 reference system, such that a users position is referenced to the WGS-84 ellipsoid. The GPS receiver collects and processes signals from the GPS satellites that are in view and then uses that information to determine and display location, speed, time, and so forth [7].

2.2 GPS OBSERVABLES

There are three GPS measurements: code pseudo range, carrier phase, and Doppler measurements. The code pseudo range is the time offset multiplied by the speed of

light and it is biased by the lack of time synchronization between the clock in the GPS satellite and the clock in the GPS receiver. It is based on observations of the time taken for the GPS signal to travel from the satellite to the antenna and it is measured through comparison of the received signal with a reference carrier generated in the receiver and modulated with a copy of C/A-code, which is unique for each satellite and is known as pseudo-random noise (PRN) code. The code pseudo range measurements contain a number of errors. The equation for the pseudo range observable between receiver i and satellite k is modeled as follows[1],[7] ,[9].

$$p_i^k = \rho_i^k + d\rho_i^k + I_i^k + T_i^k + c\delta t_i^k + \epsilon_i^k \tag{2.2.1}$$

where $p_i^k, \rho_i^k, d\rho_i^k, Ii^k, T_i^k, c\delta t_i^k$ are pseudo range, true range, the orbital error, ionospheric delay, tropospheric delay, and clock bias respectively between satellite k and receiver i. ϵ_i^k represent errors which come from pseudo range measurements and other multi path.
The carrier phase is the difference between the phase of the receiver carrier signal and the carrier received from satellite at instant measurement. The phase measurements are based on processing the reconstructed signal carriers. The received signal is demodulated through correlation between the received signal and the PRN that is generated by the receiver [1]. The measured phase consists of fractional component $\varphi(t_o)$ and integral part at an instant of reception t_o. The integral component is a number of whole wave cycles, which is measured relatively to some initial lock-on value. The receiver measures the fractional phase, and keeps track of the changes to the phase. It is more precise than the pseudo range but the problem is that the receiver cannot distinguish one cycle of a carrier from another. The initial phase is undetermined, or ambiguous, by an integer number of cycles N . This unknown quantity is the cycle ambiguity. Carrier phase can be converted into equivalent distance by similar expression as follows [1],[7] ,[9].:

$$\Phi_i^k(t) = \rho_i^k - I_i^k + T_i^k + c\delta t_i^k + \lambda N_i^k + \lambda(\varphi_i(t_o) - \varphi^k(t_o)) + \epsilon_i^k \tag{2.2.2}$$

Here, cycles phase $\Phi_i^k(t)$ is not delayed but advanced by I_i^k . Furthermore, λ is the wavelength, $\varphi(t_o)$ is the unknown fractional part of the phase near the satellite at reception, and ϵ_k is noise.
The Doppler measurement is a measure of the instantaneous phase rate and the measurement is made in the phase lock loop. It is not affected by cycle clips and does not have any

phase ambiguity. Primarily it is used for velocity estimation and expressed as follows[9]:

$$\frac{d}{dt}\Phi_i^k(t) = \frac{d}{dt}\rho_i^k + \frac{d}{dt}(d\rho_i^k) + c\frac{d}{dt}(\delta t_i^k) - \frac{d}{dt}I_i^k + \frac{d}{dt}T_i^k + \frac{d}{dt}\epsilon_i^k \tag{2.2.3}$$

where $\frac{d}{dt}\Phi_i^k(t)$, $\frac{d}{dt}\rho_i^k$, $\frac{d}{dt}(d\rho_i^k)$, $\frac{d}{dt}I_i^k$, $\frac{d}{dt}T_i^k$ *and* $\frac{d}{dt}\epsilon_i^k$ are the measured Doppler, the geometric range rate, the orbital error drift, clock error drift, the ionospheric delay drift, the tropospheric delay drift, and the noise.

2.3 GPS ERRORS

All GPS measurements, be they pseudo range or carrier phase, are affected by biases and errors which affect the accuracy of the position determination. The major error sources of the GPS measurements are signal propagation errors due to the troposphere and ionosphere effects, ephemeris errors, satellite clock errors, multi path and receiver noise errors.

2.3.1 Ephemeris Errors

The orbit quality is considered to be one of the primary accuracy limiting factors in the GPS measurements. Ephemeris errors occur when the GPS message does not transmit the correct orbital parameters. The ephemeris information used to calculate the satellite position is based on the observations from the monitor stations of the space segment. The data is processed at the Master Control Station and the satellite navigation message information is uploaded to every satellite. The ephemeris error is therefore the discrepancy between the true position (and velocity) of the satellite and its broadcast ephemeris. This grows from the time of upload by a monitor station until the next upload[10].

2.3.2 Satellite Clock Errors

Satellite clock errors arise from instabilities in the oscillators of the GPS satellites, such that ranging errors are observed in users measurements. The satellite clock error can be determined using the coefficients transmitted in the satellite navigation message. As all observation made at an instant to a particular satellite, all GPS receivers are affected by equal magnitude of the same satellite clock error, the principle of differential positioning can be used to eliminate this error (or the satellite clock error may be estimated post

mission using the precise clocks)[7],[10]. Precise clocks are computed with the precise/final orbits.

2.3.3 Receiver Clock Errors

GPS receivers are equipped with inexpensive quartz crystal oscillators with low accuracy. The offset between receiver clock time and GPS Time is the receiver clock error which affect all satellite receiver ranges measured at a particular epoch. Double differencing can be used to eliminate this error[10].

2.3.4 Multi path

Multi path is the result of GPS signals arriving at an antenna from more than one direction due to signal reflection or diffraction at various objects. Multi path effects are propagation errors arising from interference of the direct signal by reflected signals from water, metallic surfaces, and nearby buildings. The combined direct and reflected signals will give rise to incorrect pseudo range observation. Errors which arise as a result of multi path cannot be reduced by the technique of Differential GPS or DGPS, since they depend on the local reflection geometry near each receiver antenna. The multi path effects can be minimized by choosing the site of observation with minimum obstructions and reflecting surfaces nearby. Using a ground plane antenna or choke ring can minimize the multi path effects[10].

2.3.5 Ionospheric Effects

The ionosphere is [11]characterized by the presence of free electrons and positively charged atoms and molecules called ions. This is a result of the gas molecules being excited by solar radiation. The total electron content (TEC) equals the number of free electrons in the column of unit area along which the signal travels between the satellite and the receiver. TEC varies as a function of latitude of the receiver, the season, the time of the day the observation of the satellite signal is being made and the level of solar activity at the time of observation. As the electromagnetic GPS signal propagate through the medium, dispersion occurs and the free electrons delay the pseudo range and advance the carrier phase by equal magnitude. The amount is directly proportional to the TEC and inversely proportional to the carrier frequency. GPS frequency delays or advances can be

up to 50 m for signals at the zenith to as much as 150 m for observations made at the receivers horizon [12]. An effective procedure to deal with this error is to take advantage of the frequency dependence of the ionospheric effect by using a dual-frequency receiver. Measurements are made on both L1 and L2 frequency signals and combining them in a linear form, the delay is eliminated since the impact on L1 and L2 is different.

2.3.6 Tropospheric Effects

The troposphere is neither ionized nor dispersive. GPS signals traveling through this medium will experience delay that is a function of refractive index and altitude of the receiver. Since propagation of GPS signal in this medium is frequency independent, therefore this effect cannot be removed by combining observations made on L1 and L2 frequencies. Tropospheric effect is dependent on the atmospheric pressure, temperature, and humidity. The tropospheric delay is generally split into hydrostatic and wet components. The hydrostatic delay is due to the dry gases in the troposphere and the non dipole component of water vapor refractivity and can be modeled accurately using surface temperature and pressure[13]. However, the wet delay is caused by the presence of water vapor and it exists up to 10 km from the surface of the Earth. Water vapor is highly variable in space and time such that the wet delay cannot be modeled using surface measurements very accurately. Detailed discussion of the physics of the troposphere and the different troposphere models are given in Chapter 4.

Chapter 3

GAMIT/GLOBK GPS Processing Software

3.1 Introduction

GAMIT/GLOBK is a sophisticated GPS analysis package developed at MIT, the Harvard-Smithsonian Center for Astrophysics (CfA), and the Scripps Institution of Oceanography (SIO) for estimating station coordinates and velocities, stochastic or functional representations of post seismic deformation, atmospheric delays, satellite orbits, and Earth orientation parameters. GAMIT Development started in late 1970s when MIT was building GPS receivers. The Code derived from 1960-1970 Planetary ephemeris and VLBI software and Ported to Unix in 1987. Start of IGS in 1992 prompted development of automatic processing schemes[10]. The software is designed to run under any UNIX operating system supporting X-Windows. For GPS processing, the critical information needed is range and phase data from a receiver collecting data from multiple GPS satellites and information about the orbits of the satellites (earth-fixed frame) and some information about clocks in satellites. At the start of processing the analyst has available a preliminary set of station coordinates (L-file), the broadcast ephemeris (E-file or RINEX navigation file) for the satellites observed, an ensemble of phase and pseudo-range observations, and auxiliary information available from the log sheets (tracking scenarios, antenna heights, and meteorological data). In GAMIT, only crude clock information needed due to double-differencing[10].

3.2 Automatic Processing with GAMIT/GLOBK

GAMIT is composed of distinct programs which perform the major functions of preparing the data for processing (*makexp and makex*), generating reference orbits for the satellites (arc), computing residual observations (o-cs) and Modeling phase and partial derivative generation (model), GPS data cleaning and cycle slip repair (*autcln*), and performing a least-squares analysis (solve) and also minor functions of preparing are Yaw table generation for GPS satellites, Ocean tide loading coefficient generation (Explicit site values and interpolation of gridded values). Estimation of satellite and ground receiver clock models and display of phase residuals[10]. Although the modules can be run individually, they are tied together through the data flow, particularly file-naming conventions, in such a way that most processing is best done with shell scripts and a sequence of batch files set up a driver module (fixdrv) for modeling, editing, and estimation. Though the data editing is almost always performed automatically, the solution residuals can be displayed or plotted so that problematic data can be identified (cview)[10]..

Likewise, GLOBK operates through distinct programs, which can be invoked with a single command or run separately. The primary functions are to combine quasi observations either GAMIT/GLOBK h-files or the internationally accepted SINEX format from multiple networks and/or epochs (glred or globk), and to impose on this solution a reference frame appropriate to the scientific objective (glorg). A glred is used to read data from one day at a time for generating time series, while globk is for stacking multiple epochs to obtain a mean position and/or velocity.

The full sequence of steps to take you from phase data to time series is accomplished with two shell scripts: *sh_gamit* looks for raw or RINEX data over a range of days and invokes the GAMIT programs to produce constrained and loose estimates of coordinates together with sky plots of phase data as a record of the processing; *sh_glred* uses the GAMIT results to produce time series of day-to-day repeatability or a combined h-file that may be further combined with those from other epochs to estimate station velocities[10]..

3.2.1 Setup

1. The first step in running the scripts is to create an experiment directory.
2. Being on an experiment directory create working directory with a subdirectory of years.
3. Being on a year directory create a table link form ~*gg/tables*~by typing a comand

sh_setup and copy rinex, brdc and igs files.

4. On table directory edit the files $sites.defaults, sittbl., sestbl., processes.default$, copy a file $itrf08.apr$ from Chandelers MIT and creat a new station information from step 3 rinex files.

5. Finally, go to year directory by using an authomatical *sh_gamit* command run and processed the data.

3.2.2 Data Acquisition

The data is downloaded from the web site UNAVCO and uncompressed. The navigation data is discarded and precise ephemerids data is downloaded from Scripps Orbit and Permanent Array Center (SOPAC) data archives. The three IGS stations of ADIS, MAL2 and BHR1 or BHR2 tie to almost all Ethiopian GPS receiver stations are chosen. These Ethiopian GPS receiver stations are included by Crustal Movement Observation Network of Over Great Rift Valley region and managed by UNAVCO. Observation data in compressed Hatanaka format for each doy of these IGS points are also downloaded from SOPAC, UNAVCO, and CDDIS. SOPAC converts all RINEX observation files to the Hatanaka ("d file") format. RINEX files more than 60 days old are available in Hatanaka format only, so all the observation files have to be converted to RINEX format since GAMIT can only read observation and navigation files in RINEX format. This is done by using c-shell script with the name *crx2rnx* which comes with GAMIT software package. In the subsequent sections, we will describe in detailed all input files required for GAMIT processing.

3.2.3 Data Preparation for GAMIT Processing

Before processing GPS data using GAMIT, it is necessary to understand some of its file naming conventions. This assures a unique definition for each experiment, facilitates data file manage ment, and allows for ease of interactive processing and troubleshooting. First the information should be organized into sessions, defined as the spans during which all the stations tracks simultaneously the phase of two or more satellites. The main files needed for a single session processing are the RINEX observation and navigation files, station coordinates in the form of an L-file, receiver and antenna information for each site (file station.info), satellite list and scenario (file session.info), control files for the analysis (sittbl. and sestbl.) and G- and T-files from external ephemerids. Similarly, links to the

following global files are needed:

- nutations (nutabl.),
- lunar and solar ephemerides (soltab. and luntab.),
- geodetic datums (gdetic.dat),
- leap seconds (leap.sec),
- spacecraft, receiver, and antenna characteristics (svnav.dat, antmod.dat, rcvant.dat),
- Earth rotation (pole., ut1.) and
- ocean tides (stations.oct and grid.oct).

3.2.4 RINEX observation and navigation files

The RINEX observation data file (in appendix of [7]) contains the L_1 and L_2 carrier beat phases and pseudo- ranges, signal amplitudes, initial station coordinates and antenna offsets, start and stop times, and the identification of the satellites tracked in each receiver channel. The RINEX observation file name or format is seems like *siteday0.yyo*, forexampe *adis0040.11o*, which implies data from ADIS station on the day 4 of year 2011[10]. An example is given in Appendix A.4

The navigation (Broadcast Ephemeris) file consists of one or more "blocks" of orbital data as recorded by the receiver from the satellites' transmissions. For convenience we have not introduced a new format for these data; rather, they may be either in RINEX navigation file format (preferred) or in FICA format as defined by GESAR Block 9 for the TI 4100. An example, with an ephemeris block for only one satellite, is given in Appendix A.3.

3.2.5 Creating the station information file

All of the receiver and antenna information specific to a particular site occupation are recorded in the `station.info` file, which is read by makexp, makex, and model[10]. The values entered correspond to a single occupation, of either one day or a series of days. Each of the data columns must be exactly the width shown and be separated by two spaces. An example is shown in Appendix A.5.

3.2.6 Creating a scenario file

The scenario file (session.info) contains the start time, sampling interval, number of observations, and satellites ($PRN\sharp s$) to be used in generating the X-files for each day. It does not correspond to the time-dependent scenarios used to program some receiver software, but rather includes all the satellites that you want to use in the analysis generally

all available from any receiver since you can delete satellites later on in the processing. A session.info file is usually generated by a script called sh_gamit using command line arguments for the span and reading a navigation file to obtain the satellites. It can also be generated automatically to a specific experiment by the program sh_makexp using the input start/stop time and the satellites available on the navigation file[10].

3.3 Estimating a zenith delay parameter Using GAMIT

GAMIT incorporates a weighted least-squares algorithm to estimate the relative positions of a set of stations, orbital and Earth-rotation parameters, zenith delays, and phase ambiguities by fitting to doubly differenced phase observations. Since the functional (mathematical) model relating the observations and parameters is non-linear, GAMIT produces two solutions, the first to obtain coordinates within a few decimeters, and the second to obtain the final estimates. The GAMIT solution is not usually used directly to obtain the final estimates of station positions from a survey. Rather, GAMIT is used to produce estimates and an associated covariance matrix of station positions and (optionally) orbital and Earth-rotation parameters which are then input to GLOBK to estimate positions and velocities[10]. In order not to bias the combination, GAMIT generates the solution used by GLOBK with only loose constraints on the parameters, defining the reference frame only at the GLOBK stage by imposing constraints on station coordinates. Since phase ambiguities must be resolved (if possible) in the phase processing, however, GAMIT generates several intermediate solutions with user defined constraints before loosening the constraints for its final solution[10].

GAMIT allows estimation of corrections to the zenith delay. The partial derivative of phase or pseudo range with respect to the zenith delay parameter is simply the mapping function, approximately equal to the co-secant of the elevation angle of the satellite as viewed from the stations[10].

GAMIT implemented atmospheric propagation delay in the following manner[10]:

$$STD(El) = ZHD * m_h(El) + ZWDm_w(El)$$

where El is the elevation angle of the satellite, ZHD is the dry (hydrostatic) zenith delay, ZWD is the wet zenith delay, m_h is the "mapping function" for the dry delay and m_w is the mapping function for the wet delay. Both the hydrostatic zenith delay(ZHD) and the wet zenith delay (ZWD) use a Saastamoinen model. A mapping function is a mathematical model for the elevation dependence of the respective delays. The mapping

functions (for both the dry and the wet terms) are approximately equal to the cosecant of elevation, but there are significant deviations from this "co-secant law" due both to the curvature of the earth and the curvature of the path of the GPS signal propagating through the atmosphere [10].

For GAMIT the model for zenith delay can take the form of a single parameter for each station and session, or a piecewise linear function of zenith-delay over the session. In the latter case, the tabular points of the function can be constrained using a first-order Gauss-Markov process. Controls for estimation of zenith delay are input via the sestbl. and/or sittbl. See the *sestbl.* inputs, adopted as common to all stations in Appendix A.1.

3.3.1 Estimating gradients

The effects of azimuthal asymmetry in the atmospheric delay are not included in model but may be estimated in solve. The coded partials imply a model of the form[10]:

$$ATDEL(EL, AZ) = GRADNS*AZMAP(EL)*cos(AZ)+GRADEW*AZMAP(EL)*sin(AZ)$$

where EL is the elevation angle, AZ the azimuth, and AZMAP the mapping function for gradients, given by[10]:

$$AZMAP = 1./(sin(EL) * tan(EL) + C)$$

and C is a constant equal to 0.003[10]. Since the gradient parameters, GRADNS and GRADEW have small and non-intuitive values near the zenith (i.e., for AZMAP = 1), we rescale them to represent the difference between the the north (or east) and south (or west) delay at 10 degrees elevation[10].

3.3.2 Extracting estimates of ZTDs and precipitable water

The utility metutil, invoked by *sh_metutil* allows to extract the zenith delay estimates from the solve o-file under each day of year directory, apply corrections for the hydrostatic delay, and convert the residual wet delay to precipitable water. The source of the hydrostatic corrections can be the pressure values input to model as apriori. In the first instance, the command line has the following form[10]:

$$sh\_metutil - foexpta.021 - zzadis8.021$$

An example of meteorological output are given in Appendix B.

Chapter 4

TROPOSPHERIC DELAY MODEL

4.1 INTRODUCTION

Now a day, there are several types of common troposphere delay correction models that have been reported in the scientific literature, such as Saastamoinen, Hopfield, Chao model, Egnos models, UNB3m (University of New Brunswick modified) model, EGNOS(European Geostationary Navigation Overlay Service) model.
In this chapter, we present a general overview of the structure of the troposphere, the effect of neutral atmosphere on electromagnetic wave with the tropospheric refractive index, and we review a very significant number of troposphere delay models reported in the scientific literature in the last few decades.

4.2 TROPOSPHERE AND ITS STRUCTURE

The atmosphere of the earth is categorized into different layers according to their physical properties and influences on to the electromagnetic waves. Based on the electromagnetic wave, the atmosphere is splited in to the neutral atmosphere and the ionosphere.
The ionosphere is the upper part of the atmosphere, which is responsible for the absorption and reflection of radio waves at low frequencies (generally below 25 MHz)[1] where solar radiation (predominately by ultra-violet radiation) results in ionization and diversity that varies as a function of the time of day. It is characterized by its free, neutral, and charged particles. Molecules and atoms in the upper atmosphere are ionized by absorbing radiation energy from the Sun. Free electrons and ions in the ionosphere are also attributed to ion exchange between the ionosphere and the plasma sphere above it[11]. While the neutral

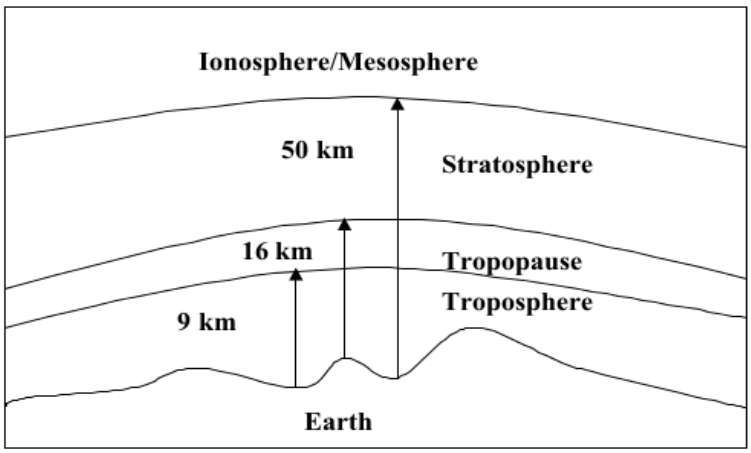

Figure 4.1: Vertical structure layer of the atmosphere.

atmosphere refers to the non-ionized portion of the atmosphere, which comprises of the troposphere and the stratosphere and it extends from the earths surface to about 50 km height. The troposphere makes up the lower portion of the neutral atmosphere, extending from the earths surface upto an altitude of approximately 16 kilometers at the equator and 8 kilometers at the poles. The stratosphere extends upwards from the tropopause to approximately 50 kilometers in altitude. The neutral atmosphere consists of a combination of several gases such as N_2 (78.09 %), O_2 (20.95 %), Ar (0.95 %) [1].

4.3 TROPOSPHERIC EFFECTS ON GPS SIGNAL AND REFRACTIVITY

4.3.1 Electromagnetic Wave Propagation in the Troposphere

Satellite navigation and positioning relies on electromagnetic waves, whose characteristics are described by Maxwells equations. Oscillating electric or magnetic forces generate the waves. The duality of electromagnetic waves manifests itself in the combined propagation of an electric field and a magnetic field[14]. An oscillating electric field causes a magnetic field through magnetic flux. In homogeneous, isotropic, and stationary media, which are media that do not show any spatial or temporal variations of their physical properties, the electric field vector E and the magnetic field vector B are orthogonal to each other and also orthogonal to the propagation direction of the electromagnetic wave[1].

The speed of propagation of an electromagnetic wave may be considered to be constant

and equal to the speed of light in free space, c. However, because of many constituents of air molecules, the neutral atmosphere is inhomogeneous medium and totally different from free space. It changes in the speed and in direction of electromagnetic signal propagation in the medium.

The electromagnetic field are described by Maxwell's equations[14]

$$\nabla \cdot D = \rho \tag{4.3.1}$$

$$\nabla \cdot B = 0 \tag{4.3.2}$$

$$\nabla \times E + \frac{\partial}{\partial t} B = 0 \tag{4.3.3}$$

$$\nabla \times H = J + \frac{\partial D}{\partial t} \tag{4.3.4}$$

where E is the electric field, $D = \epsilon_o E + P$ is the electric displacement field, ϵ_o is the permittivity of vacuum, ρ is the charge density and P is the polarization. B is the magnetic field described by the magnetic induction, the magnetic field $H = \frac{1}{\mu_o B} - M$, the magnetization M and permeability of free space μ_o, J is the current density vector. In the neutral atmosphere the magnetization M, the charge density ρ and current density$J$ vanish[15]. The interaction of electromagnetic field with propagation medium is caused only by the electric field E which polarizes the air molecules[15],[16]. This process is described by the dielectric susceptibility η define a relationship between a molecular polarization P and applied electric field E[14]:

$$P = \eta E \tag{4.3.5}$$

When electromagnetic wave interact with neutral atmosphere or tropospheric constituents, molecules get polarized due to charged particles (electrons and protons). Molecular polarization yields non-vanishing refractivity for all types (wet and dry) of molecules and is caused by the electrical field which shifts the negatively charged elevation cloud with in the molecule and produces an induced dipole moment P for each single molecule[3],[15] ,[16]. From equation (3.3.5) we define the linear relationship between displacement electric field and electric field[14]:

$$D = \epsilon_o E + P = \epsilon_o E + \eta E = \epsilon_o E(1 + \frac{\eta}{\epsilon_o}) \tag{4.3.6}$$

$$D = \epsilon \epsilon_o E \tag{4.3.7}$$

where $\epsilon = 1 + \frac{\eta}{\epsilon_o}$ is the dielectric permittivity.
The curl of Equation number (4.3.3) will give as

$$\nabla \times \left((\nabla \times E) + \frac{\partial B}{\partial t} \right) = 0$$

$$\Rightarrow \nabla \times (\nabla \times E) + \frac{\partial}{\partial t}(\nabla \times B) = 0$$

$$\Rightarrow \nabla(\nabla \cdot E) - \nabla^2 E + \frac{\partial}{\partial t}(\nabla \times B) = 0 \tag{4.3.8}$$

Now for free space($\rho = 0, J = 0$) substituting equation number (4.3.4) into the above equation number (4.3.8) will give a general solutions of Maxwells equation as linear combinations of single-frequency solutions:

$$\nabla^2 E - \mu_o \epsilon_o \frac{\partial^2 E}{\partial t^2} = 0 \tag{4.3.9}$$

and in similar manner

$$\nabla^2 B - \mu_o \epsilon_0 \frac{\partial^2 B}{\partial t^2} = 0 \tag{4.3.10}$$

Thus, to separate the space and time dependence in Maxwell's equation we assume that all fields have a space and time dependence:

$$E(r,t) = E_o e^{i[n(r)k \cdot r - \omega t]} \tag{4.3.11}$$

$$B(r,t) = B_o e^{i[n(r)k \cdot r - \omega t]} \tag{4.3.12}$$

where the $\omega = 2\pi f$ is the angular frequency, k is a vector normal to the wave front magnitude equales to $\frac{2\pi}{\lambda}$. The value of n(r) represents the refractive index at the point r(x,y,z). In free space, the speed of propagation of electromagnetic waves is given by[14]

$$c = \frac{1}{\sqrt{\epsilon_o \mu_o}} \tag{4.3.13}$$

where c is a constant and called speed of light ($\tilde{}3\times10^8 ms^{-1}$), However, when electromagnetic wave propagate through different medium, such as air and water vapors, they no longer propagate at c, but at slower velocity that is related to the permittivity, ϵ, and magnetic inductive capacity, μ of the medium. The velocity of an electromagnetic wave in medium other than a vacuum is given by

$$v = \frac{1}{\sqrt{\epsilon \mu}} \tag{4.3.14}$$

where the magnetic permeability μ is approximately 1 for air.

4.3.2 Refractive Index And Refractivity in the Troposphere

The change in velocity of propagation changes and delay of the signal transit time and, therefore, delay of the apparent range of satellite, which is the basic measurement from GPS. Radio signal propagating in the Earth's environment are reflected by the ground, buildings, and surface of water, as much as light is reflected. The atmosphere changes the velocity (speed and direction) of propagation of radio signal. This phenomenon is referred to as refraction. Refraction describes the change of propagation direction when a wavefront passes from one to the other medium. When radio signals propagate through the atmosphere, they are delayed due to the different refractivity indexes of each layer of the atmosphere. The atmosphere has a significant effect on the propagation of a GPS signal. According to Snell's law, the sine of the angle of incidence, β_i, and the sine of the angle of refraction, β_r, define a constant ratio[17].

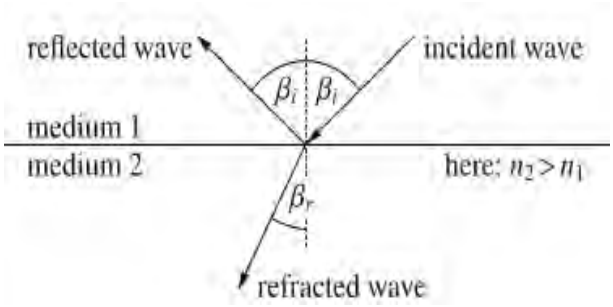

Figure 4.2: Reflection and refraction of an electromagnetic wave

$$\frac{sin\beta_i}{sin\beta_r} = \frac{n_2}{n_1} = constant \tag{4.3.15}$$

The refractive index n_i of medium is defined as the ratio of the speed of propagation of an electromagnetic wave in vacuum (which is a universal constant), c, to the phase velocity v_i of propagation in the medium :

$$n_i = \frac{c}{v_i} \tag{4.3.16}$$

Snells law, thus, can be written in the form

$$n_1 v_2 = n_2 v_2 = c \tag{4.3.17}$$

Starting from the top, the signals first passe through the ionosphere, where due to the existence of free electrons (presence of ionized gas molecules) ionospheric delay occurred

and the refractive index is smaller than unity. When the signal reaches the neutral atmosphere, which is composed of different atmospheric gases (temperature, pressure, humidity, ...) tropospheric delay occurrs for refractive index is greater than unity. The refractive index is related to the density of molecules and their polarization. The density of atmosphere generally decreases exponentially with height from sea level to the top of atmosphere. However, the rate at which density varies with height is modified by the presence of inversion layers, since density depends on pressure and temperature[1].

Molecules which have a non-vanishing permanent electric dipole moment, like water molecule, show an additional effect. The electric field tends to line up the permanent dipole moment of the molecules, which are distributed due to thermal motion if no field is applied[1]. The water vapor molecules in atmosphere are polar in nature possessing permanent dipole moment[16]. Each polar molecule represents a dipole. In the absence of electric force, such as that induced by propagating microwaves from GPS signal causes the dipole field to align, and add constructively to the net electric force acting on each molecules[1],[3]. The electric force acting on each molecule is the sum of the external electric force and the electric force produced by each of the polar molecules[1]. Gradients of water vapor molecules act to bend a propagating electromagnetic wave, much as a prism bends visible lights[3],[16].

In the troposphere, the refractive index is influenced by temperature, pressure and water vapor. The refractive index, n, expressed as in terms of temperature, T, the partial pressure of dry air, P_d, and water vapor pressure, P_w, is discussed by Battan [18] and Doviak and Zrnic [19] and given by

$$n = 1 + (k_1 \frac{P_H}{T} + k_2 \frac{P_w}{T} + k_3 \frac{P_w}{T^2}) 10^{-6} \tag{4.3.18}$$

where $k_1 = 77.604 \frac{K}{Pa}$, $k_2 = 64.79 \frac{K}{Pa}$, $k_3 = 377600.0 \frac{K^2}{Pa}$. The refractive index of a neutral atmosphere of moist air is different from unity because its constituents suffer polarization induced by the electromagnetic field of the radio signals[2]. A permanent dipole moment of water vapor molecules induced polarization and produces an orientation effect, which contributes significantly to the variations of the refractive index. The dry constituents have no permanent dipole moment, but their molecules are displaced under the influence of the electromagnetic field and a dipole moment is generated[1]. As the electromagnetic waves in the atmosphere propagate just slightly slower than in a vacuum, refractive index

is more conveniently expressed by another quantity, refractivty, N, as [7]

$$N = (n-1)10^6 \tag{4.3.19}$$

Now substituting equation (4.3.18) in to the equation (4.3.9) we have

$$N = k_1\frac{P_d}{T} + k_2\frac{P_w}{T} + k_3\frac{P_w}{T^2} \tag{4.3.20}$$

The refractive index can be expressed as the sum of the hydrostatic or dry and non-hydrostatic or wet refractivities:

$$N = N_H + N_W$$

where $N_H = k_1\frac{P_d}{T}$ is the hydrostatic or dry and $N_w = k_2\frac{P_w}{T} + k_3\frac{P_w}{T^2}$ is non-hydrostatic or wet refractivities. These two components have different effects on the propagation of the GPS signal. The hydrostatic component contributes to approximately 90 percent of the total tropospheric delay. It can be modeled pretty accurately by using surface meteorological parameters[20]. The wet component is much more difficult to model efficiently, as the variation of water vapor in the atmosphere varies greatly with time and location.

4.4 Revision of Tropospheric Delay Model

4.4.1 Saastamoinen model

Saastamoinen model[20] is given as a function of latitude, altitude, satellite elevation, temperature, and water vapor pressure of the station. The refractivity can alternatively be deduced from gas laws. The hydrostatic (ZHD) and wet (ZWD) components of the delay in the zenith direction are expressed as:

$$ZHD = 0.002277(1 + 0.0026cos2\varphi + 0.00028h)P_o$$

$$ZWD = 0.002277\left(\frac{1255}{T} + 0.05\right)P_w$$

where P_0 is the surface pressure in millibars, T_0 is the surface temperature in Kelvin, p_w is partial pressure of water vapor in millibars , φ is the latitude of the receiver in radians, and h is the altitude above ellipsoid surface. The hydrostatic delay model may

be expressed simply as a function of measured surface pressure. In Saastamoinen models the total tropospheric zenith delay expressed in meters as[5],[20]

$$ZTD = 0.002277 \times \frac{[P_o + (0.05 + \frac{1255}{T_o+273.15})P_w]}{f(\varphi, h)}$$

where

$$P_w = rh \times 6:11 \times 10^{[\frac{7.5T_o}{T_o+273.15}]}$$

$$f(\varphi, h) = 1 - 0.00266cos2\varphi - 0.00028h$$

and rh is the relative humidity. A numerical assessment using parameters of a standard atmosphere at sea level (p = 1013.25 millibar, T = 273.16 kelvin, and P_w=0 millibar) results in a tropospheric zenith delay of about 2.3 m [1].

4.4.2 Hopfield model

Hopfield model is given as using[1],[21] a representation of the dry refractivity as a function of the height h above the surface by

$$N_H(h) = N_{H,o}\left[\frac{h_H - h}{h_H}\right]^4$$

under the assumption of a polytropic layer with thickness

$$h_H = 40136 + 148.72(T - 273.16) \quad [m]$$

Here, the hydrostatic tropospheric path delay can be solved as integral of the dry refractivty along the vertical direction and if the curvature of the signal path is neglected:

$$ZHD = 10^{-6}N_{H,o}\int_0^{h_H}\left[\frac{h_H - h}{h_H}\right]^4 dh$$

where the lower limit $h = 0$ corresponds to an observation site on the surface of the earth and where the constant denominator has been extracted. After integration, the dry portion of the tropospheric zenith delay is given by

$$ZWD = 10^{-6}N_{H,o}\frac{1}{h_H^4}\left[-\frac{1}{5}(h_H - h)^5\Big|_0^{h_H}\right]$$

$$= \frac{10^{-6}}{5}N_{H,o}h_H$$

For wet portion, Hopfield model assumes the same functional model for both the wet and dry components. Thus,

$$N_w(h) = N_{w,o}\left[\frac{h_w - h}{h_w}\right]^4$$

where the mean value $h_w = 11000m$ is used. Sometimes other values such as hw = 12 000 m have been proposed by Bernhard [1] . Now in similar manner as in the above steps integration, the wet portion of the tropospheric zenith delay is

$$ZTD_w = \frac{10^{-6}}{5} N_{w,o} h_w$$

Therefore, the total tropospheric zenith delay is given by:

$$ZTD = ZHD + ZWD = \frac{10^{-6}}{5}[N_{H,o}h_H + N_{w,o}h_w]$$

4.4.3 Chao model

In 1971, Chao derived a zenith wet delay model based upon the application of the hydrostatic law to the water vapor, and the ideal gas law [Chao, 1971a][22]. As these assumptions lead to unreasonable results when compared against radiosonde data. Chao replaced the ideal gas law equation of state by the adiabatic law:

$$P_w = k^\beta \rho_w^\beta$$

where k is Boltzmann constant, ρ is the specific heat ratio ($\sim$ 1.3 for water vapor).The followng expression [Chao,1973][23] for wet delay:

$$ZWD = 4.70 \times 10^2 \frac{P_{wo}^{1.23}}{T_o^2} + 1.71 \times 10^6 \frac{P_{wo}^{1.46}}{T_o^3}\alpha$$

where α is the temperature lapse rate. This model is not very sensitive to the temperature lapse rate and the use of a mean value of α (e.g. $0.0065Kkm^{-1}$).

4.4.4 Ifadis model

Ifadis (1986) developed empirical model for the zenith wet delay based on the fact that there is a linear correlation between the zenith wet delay and the surface meteorological parameters [24]. The zenith wet delay model is given by the following expression:

$$ZWD = 0.00554 - 0.880 \times 10^{-4}(P_s - 1000.0) + 0.272 \times 10^{-4} P_{ws} + 2.771\left[\frac{P_{wo}}{T_o}\right]$$

4.4.5 Berman Model

The Berman model (1976) [25] is based on the existence of a strong correlation between the ratios of the wet and zenith hydrostatic delays and the corresponding refractivities:

$$\frac{ZWD}{ZHD} = K \times \left[\frac{N_w}{N_H}\right]$$

where K is a constant and is determined with empirical values. The zenith wet delay model can be expressed by the following expression:

$$ZWD = 10.946\left[\frac{P_{ws}}{T_s}\right]$$

4.4.6 UNB Neutral Atmosphere Models

The UNB neutral atmosphere models [26] computes the hydrostatic and wet zenith delays according to Saastamoinen model prediction of the meteorological parameters with annual mean and amplitude for temperature, pressure and relative humidity. In this model, the pressure, temperature, water vapor pressure, temperature lapse rate β, water vapor pressure decline rate λ, and the average value of these five meteorological parameters are provided on the mean sea level for each latitude band.
The zenith delays can be computed according to [26]

$$ZHD = \frac{10^{-6}k_1 R}{g_m} \cdot P_o \cdot \left[1 - \frac{\beta h}{T_o}\right]^{\frac{g}{R\beta}}$$

and

$$ZWD = 10^{-6}R\frac{(T_m k_2^{'} + k_3)}{g_m \lambda^{'} - \beta R} \cdot \frac{P_{wo}}{T_o} \cdot \left[1 - \frac{\beta h}{T_o}\right]^{\frac{\lambda^{'} g}{R\beta} - 1}$$

where T_o, P_o, P_{wo} are the surface temperature, pressure, and water vapor pressure respectively. And h is the orthometric height in m, R is the gas constant for dry air ($287.054 Jkg^{-1}K^{-1}$), g_m is the acceleration of gravity at the atmospheric column and can be computed from

$$g_m = 9.784(1 - 2.66 \times 10^{-3} cos(2\varphi) 2.8 \times 10^{-7} h)$$

where T_m is the mean temperature of water vapor in K and can be computed from

$$T_m = T\left[1 - \frac{\beta R}{g_m \lambda^{'}}\right]$$

$$\lambda^{'} = \lambda + 1$$

Chapter 5

Methodology

5.1 Adaption of SHAO-C Tropospheric Delay Model over Ethiopia

Troposphere delay modeling is important for the accuracy of navigation and positioning applications of GPS signal in the neutral atmosphere. Precise GPS applications are complicated by atmospheric effects. The effect of gravity causes the atmosphere to be generally more dense and moist at lower altitudes than at higher ones. Though the effect is small, it causes a significant bending of the propagated signal path under many conditions. Signal propagation in the Earths atmosphere can be very complicated depending upon the signal frequency and the environment. The GPS signal travels a distance ranges that from about 20,000km when satellite over head to about 26,000km when it is rising or setting. All but the final 5 percent of the signal travel can be regarded as in vacuum or free space[7].

As we mention in chapter three the refractive index within the neutral atmosphere plays an important role in the propagation of radio waves. The tropospheric delay is due to the excess path delay and the bending effects in the neutral atmosphere of the radio signal. The refractive index of the troposphere is greater than unity causing an excess delay of the signal, and the change in the refractive index with height causes the bending of the signal[17]. On other hand, the continuous variation of the refractive index causes a deviation of its trajectory from a straight line.

In free space, the actual time along the direct signal path[7]:

$$\tau = \frac{1}{c}\int dh \tag{5.1.1}$$

On the other hand, for a given refractive index profile variation along the propagation path of signal (along the electromagnetic path of signal), the real time of signal is defined as

$$\tau' = \frac{1}{c}\int n(h)dh \tag{5.1.2}$$

where $n(h)$ is the refractive index along the signal propagation path, and dh is a differential element of length along the ray path. Thus, the change of real time with actual time is described as

$$\Delta\tau = \frac{1}{c}\int (n-1)dh \tag{5.1.3}$$

The zenith tropospheric delay is directly proportional to the refractive index or refractivity and can be expressed as a function of atmospheric temperature, pressure and humidity. The tropospheric delay can be computed through the integration along the signal path through the troposphere, or as the difference between the electromagnetic path length and the geometric path length using following expression[7],[17]:

$$ZTD = c\Delta\tau = \int_{path} (n-1)dh \tag{5.1.4}$$

5.2 Algorithm and Methodology

The weather model used for this study is provided by the ECMWF. The ECMWF model is a global model and consists of a general circulation model and a data assimilation system [27]. For this thesis we used analysis field of the surface pressure P_s, the geopotential at the Earth's surface , Φ, the temperature, T, and the specific humidity q.

These field are extract for each grid cell of latitude, λ_i, and longitude, ϕ_j, for the period under study. The ERA-Interim data covering $3^o - 17^o$N and $33^o b - 48^o$ E at horizontal resolution of 0.75 degree and temporal resolution of 6 hrs is used in this study. The refractivity, N, can be calculated for each grid cell and pressure level h_k as

$$\begin{aligned} N_k(\lambda_i,\phi_j,h_k) &= k_1\frac{(P(\lambda_i,\phi_j,h_k) - P_w(\lambda_i,\phi_j,h_k))}{T(\lambda_i,\phi_j,h_k)} + k_2\frac{P_w(\lambda_i,\phi_j,h_k)}{T(\lambda_i,\phi_j,h_k)} + k_3\frac{p_w(\lambda_i,\phi_j,h_k)}{T^2(\lambda_i,\phi_j,h_k)} \\ where & \\ P_w(\lambda_i,\phi_j,h_k) &= \frac{q(\lambda_i,\phi_j,h_k) * P(\lambda_i,\phi_j,h_k)}{0.622} \end{aligned} \tag{5.2.1}$$

following equation (4.20).

The variable P represents air pressure in pascal (Pa), T is the temperature in Kelvin

(K) and P_w is the partial pressure of water vapor in pascal (Pa) and N represent the refractivity.

The reference height (surface reference height) is obtained from high resolution digital elevation model (DEM). From equation (5.1.4) the troposphere zenith delay of the integration part can be discretized as follows[4],[5]:

$$ZTD = 10^{-6} \int_{h_{bot}}^{h_{top}} N dh = 10^{-6} \sum_{k=0}^{l} N_k \Delta h_k \tag{5.2.2}$$

where l is the total vertical layer of troposphere and k is index of the layer.

When the troposphere is in hydrostatic equilibrium, the thickens height Δh_k is given as[17]

$$g\rho dh + dP = 0$$

and the delay is

$$ZTD(\lambda, \phi, h, t) = \frac{10^{-6}}{g\rho} \int_{h_{top}}^{h_{bot}} N dP = \frac{1}{g\rho} \sum_{k=0}^{l} N_k \Delta P_k \tag{5.2.3}$$

where ρ is the density of troposphere.

Here the functional relationship describing vertical variation (altitude variation) in the total zenith delay, is given using a direct second order polynomial fitting, expressed as

$$ZTD(\lambda, \phi, h, t) = ZTD(\lambda, \phi, h_o, t)) + \left[\frac{\partial ZTD(\lambda, \phi, h, t)}{\partial h}\bigg|_{h_o} (h - h_o) + \frac{\partial^2 ZTD}{\partial h^2}\bigg|_{h_o} (h - h_o)^2 \right] \tag{5.2.4}$$

where h_o and h are the reference height and the users height, respectively.

This also can be rewritten as [4]

$$ZTD(\lambda, \phi, h, t)) = ZTD(\lambda, \phi, h_o, t)) + a_1(h - h_o) + a_2(h - h_o)^2 \tag{5.2.5}$$

where

$$\begin{aligned} a_1 &= \frac{\partial ZTD}{\partial h} \qquad \textit{is the decreasing rate and} \\ a_2 &= \frac{\partial^2 ZTD}{\partial h^2} \qquad \textit{is acceleration rate of ZTD.} \end{aligned}$$

Based on the analysis of the temporal and spatial characteristics of ZTD, the zenith delay at the surface can be estimated for desired day of year using harmonic function analysis

as follows:

$$\begin{aligned} ZTD(\lambda_i, \phi_j, h_{oij}, t)) &= ZTD_{mean}(\lambda_i, \phi_j, h_{oij}) - \\ & \quad ZTD_{amp}(\lambda, \phi) cos[2\pi \frac{(t - t_{min})}{365.25}] \end{aligned} \tag{5.2.6}$$

where the reference height h_{oij} is the average surface height of each grid (obtained from high resolution digital elevation model (DEM)) in km, $ZTD_{mean}(\lambda, \phi, h_{oij})$ is the average zenith delay on average height at each grid in meter, $\Delta ZTD_{amp}(\lambda, \phi)$ is the amplitude of zenith delay on average height at each grid in meter. Finally the model defines the total zenith delay as

$$\begin{aligned} ZTD(\lambda_i, \phi_j, h_{oij}, t)) &= ZTD_{mean}(\lambda_i, \phi_j, h_{oij}) - ZTD_{amp}(\lambda, \phi) cos[2\pi \frac{(t - t_{min})}{365.25}] \\ &+ a_1(h - h_o) + a_2(h - h_o)^2 \end{aligned} \tag{5.2.7}$$

The precipitation water (PW) derived from Zenith wet delay is given by [6]:

$$PW = \Pi * ZWD \tag{5.2.8}$$

where Π is a dimensionless conversion factor

$$\Pi = \frac{10^6}{\rho_v R_v (\frac{k_3}{T_m} + k_2 - \frac{R_d}{R_v} k_1)}$$

where ρ_v is density of water vapor, R_v is specific gas constant of water vapor, R_d is specific gas constants of dry air and T_m is the mean temperature. The mean temperature T_m is well approximated by surface temperature measurements using the empirical formula[2],[10] as follows:

$$T_m \approx 70.2 + 0.72 T_s$$

where T_s is surface temperature in Kelvin.

Chapter 6

RESULT AND DISCUSION

This chapter presents the final results of the modified SHAO-C tropospheric delay correction model for Ethiopia and its neighbors of ZTDs. To validate a tropospheric delay correction model over Ethiopia regional characteristics, we discussed and compared the importance of continuous time series of the measured ZTDs at several GPS stations from the Crustal Movement Observation Network of over Great Rift Valley regions of Eastern Africa base stations which are managed by UNAVCO (Figure 6.1). We analyzed the GPS data from

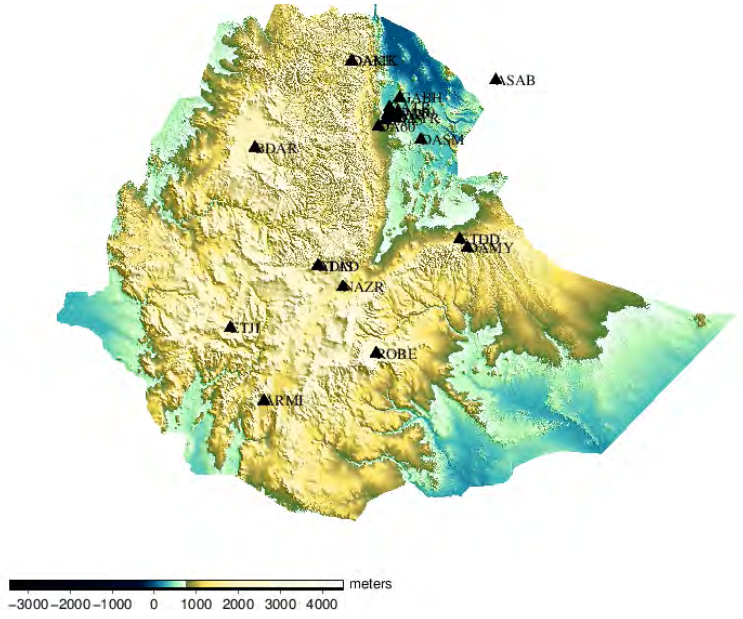

Figure 6.1: GPS stations over Ethiopia and its neighbors

years 2007 to2011. The GAMIT software was used to process the GPS data, which parameterizes ZTD as a stochastic variation from the Vienna Mapping Function 1 (VMF1)

model and the ZTDs are calculated at a 2 hours interval for each station with piecewise linear interpolation (PWL).

6.1 Characteristics of ZTD Over Ethiopia

The GPS ZTD time series have been analyzed for 5 years for the majority of the 15 sites of the network. Figure 5.2 indicates that the time series of ZTDs exhibit the well known annual signal, which can be described by a cosine function. Clearly the ZTD depends on the altitude. In low land stations (such as Asab (ASAB), Semera (DASM)) the magnitude of ZTD is much higher compared to that of high land station (such as Robe (ROBE), Addis Ababa (ADIS)). On the other hand, from Table 5.1 the seasonal ZTD shows an apparent variation with lower values in the winter and higher values in the summer months, which reflects that in summer season due to strong moisture field (high water vapor pressure) the ZTD magnitude is higher. The minimum mean annual average value of ZTDs, ZTD_{mean}, is 1.8491 at Addis Ababa (ADIS) station, and the maximum is 2.5045 at Asab (ASAB) station. The mean annual amplitude variation of ZTD given in equation (5.2.6)ranges from 0.03 m to 0.06 m depending on the site, with most sites around 0.031 m to 0.036 m.

ZTDs very spatial mainly along altitude, though there is slight variation along both latitude and longitude over Ethiopia. For instance, the magnitude of ZTD is greater along the Rift Valley at Asab and Semera station.

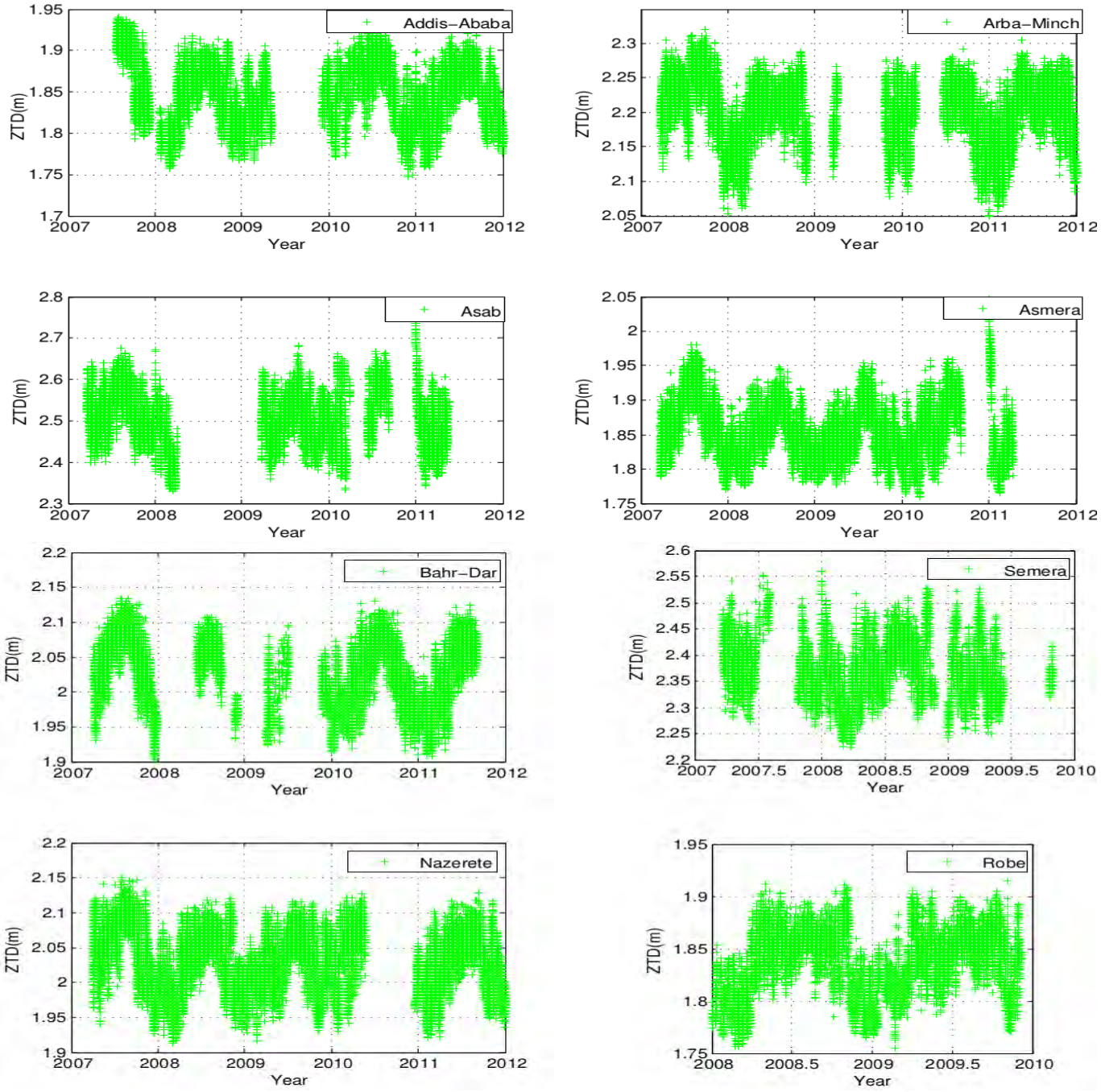

Figure 6.2: Time series of ZTDs over Addis Ababa (ADIS), Arba Minch (ARMI), Asab (ASAB), Asmera (ASMA), Bahr Dar (BDAR), Robe (ROBE), Semera (DASM) and Nazereth (NAZR) GPS receiver sites. There are data gaps of different lengths at most of GPS stations.

Table 6.1: The seasonal mean value of ZTD and annual mean ZTD (in meter) at Addis Ababa(ADIS), Arba Minch (ARMI), Asab (ASAB), Asmera (ASMA), Bahr Dara (BDAR), Alemeya (DAMY), Semera (DASM) and Nazereth (NAZR) GPS stations

Site	lat (deg)	long (deg)	Altit (m)	ZTD (Spr)	ZTD (Sum)	ZTD (Aut)	ZTD (Wint)	Amplitude (ZTD_{amp})	Average (ZTD_{mean})
ADIS	8.970	38.740	2439.9	1.8433	1.8726	1.8440	1.8228	0.0313	1.8491
ARMI	6.022	37.561	1199.9	2.1993	2.2221	2.2167	2.1646	0.03676	2.2027
ASAB	13.063	42.654	8.96	2.5022	2.5261	2.4775	2.4954	0.0527	2.5045
ASMA	15.34	38.91	2321.9	1.8386	1.8822	1.8394	1.8186	0.0335	1.8540
BDAR	11.524	37.356	1793.9	2.0053	2.12653	2.0152	1.9692	0.0415	2.0272
DAMY	9.360	42.034	2042.4	1.9349	1.9754	1.9239	1.9126	0.0363	1.9414
DASM	11.779	41.09	418.34	2.3338	2.4179	2.3872	2.2691	0.0469	2.3721
NAZR	8.568	39.291	1722.6	2.0262	2.1577	2.0273	1.9856	0.0361	2.0326

6.2 Establishment of the Model Parameters

In this Section we determine the model coefficients, and analyze its temporal and spatial characteristics over the region. The model parameter average value are determined at each grid point by fitting equation (5.2.4) to observations. The model daily variations parameter at each grid point of day of years also harmonically fitting equation (5.2.5) to observations.

6.2.1 Determination of the Model coefficients

The following four parameters of model coefficients (the average zenith delay ZTD_{mean}, the amplitude zenith delay ZTD_{amp}, the decreasing rate a_1, and the accelerating rate a_2 except the average surface height h_o) are derived from using a 6-hour interval ERA-Interim pressure level atmospheric data. The altitude (the average surface height h_o) in each grid is obtained from high resolution digital elevation model (DEM) (Figure 6.3). The variation of the average ZTD_{mean} (Figure 6.4) and ZWD_{mean} (Figure 6.5) at average height h_o have inverse relationship with the average height h_o (i.e in the central and northern part of Ethiopia, which is the high land region, the magnitude of the delay is small). The decreasing rates a_1 (Figure 6.8, Figure 6.9) have the similar shape as the average surface height h_o, which reflects the decreasing variation of atmosphere density with the increasing altitude.

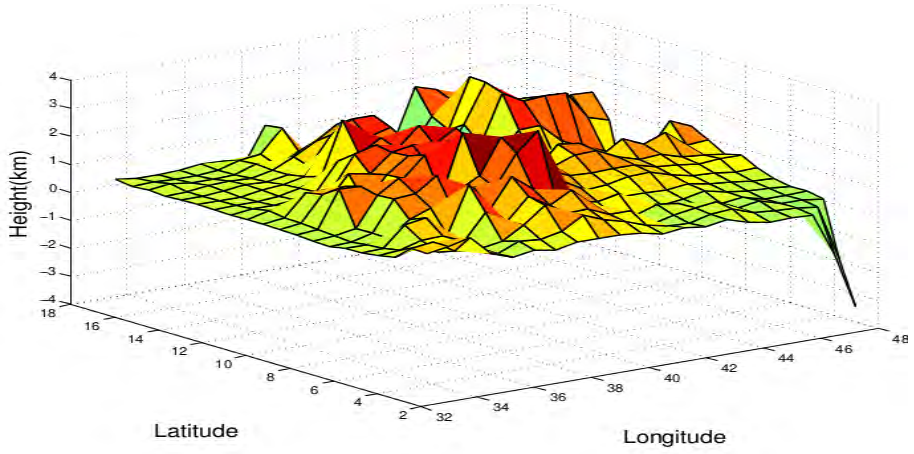

Figure 6.3: Average height ho in each grid of the model over Ethiopia and its neighbors.

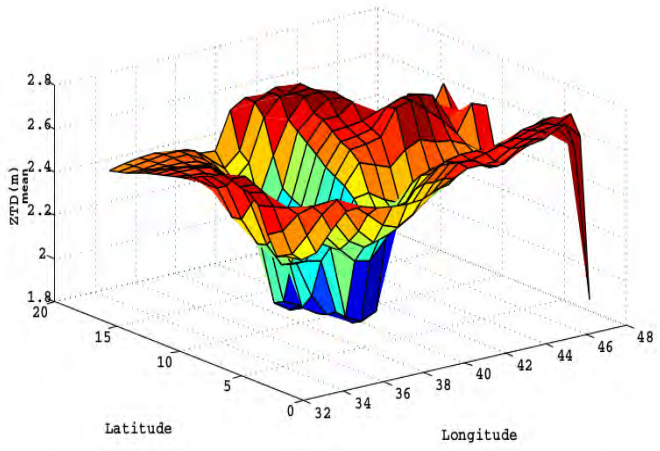

Figure 6.4: Average ZTD_{mean} in each grid of the model over Ethiopia and the its neighbors.

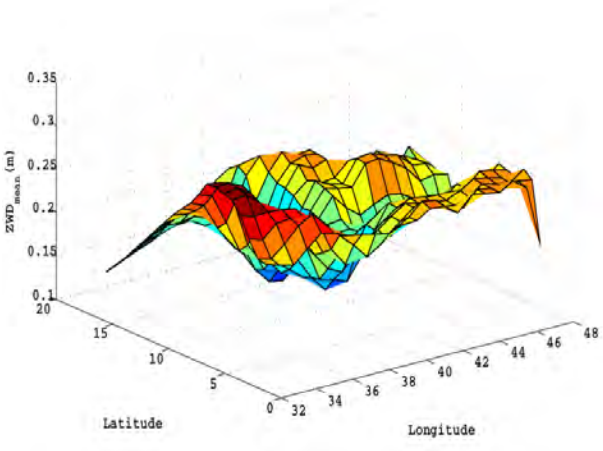

Figure 6.5: Average ZWD_{mean} in each grid of the model over Ethiopia and the its neighbors.

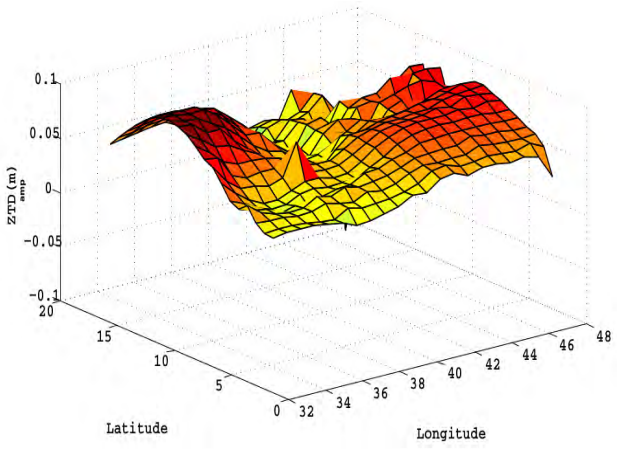

Figure 6.6: ZTD amplitude ZTD_{amp} in each grid of the model over Ethiopia and its neighbours.

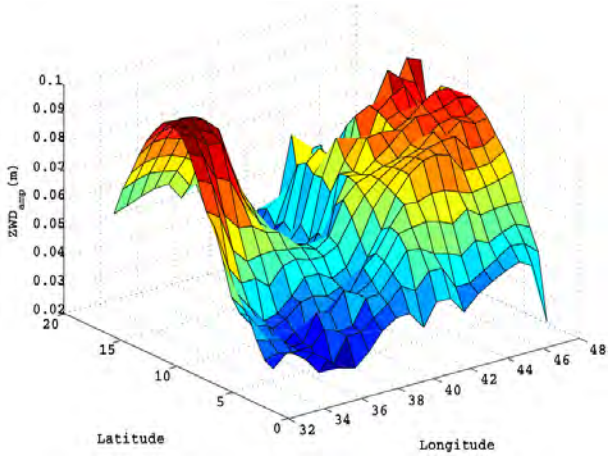

Figure 6.7: ZWD amplitude ZWD_{amp} in each grid of the model over Ethiopia and its neighbours.

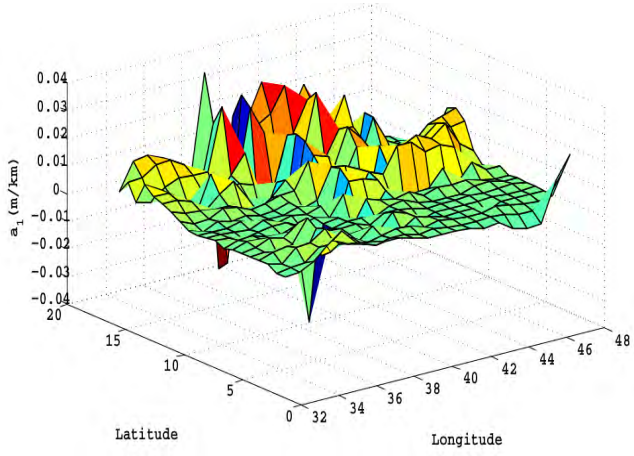

Figure 6.8: The ZTD decreasing rate a_1 determined from the model during 26-July,2010 - 06-August,2010 in summer season over Ethiopia and its neighbors.

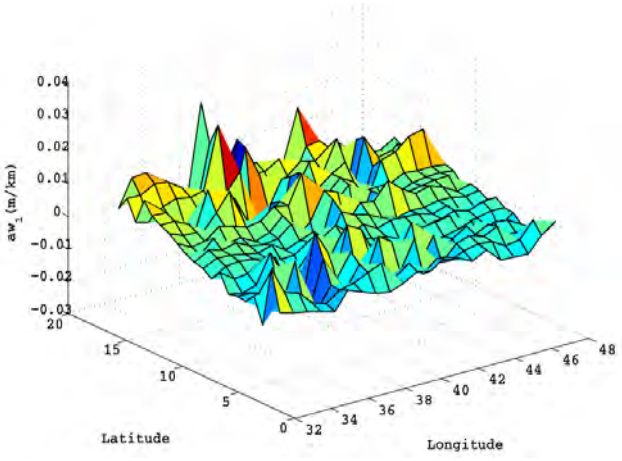

Figure 6.9: The ZWD decreasing rate aw_1 determined from the model during 26-July,2010 - 06-August,2010 in summer season over Ethiopia and its neighbors.

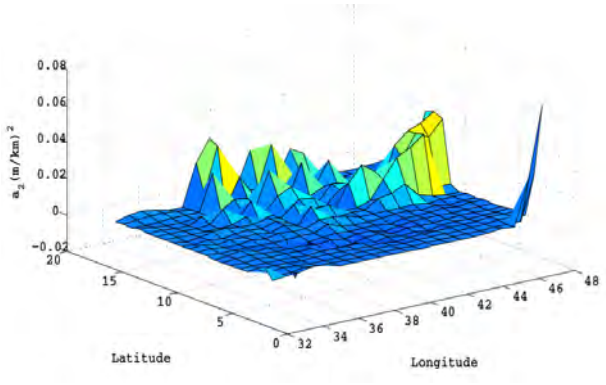

Figure 6.10: The ZTD accelerating rate a_2 determined from the model during 26-July,2010 - 06-August,2010 in summer season over Ethiopia and its neighbors.

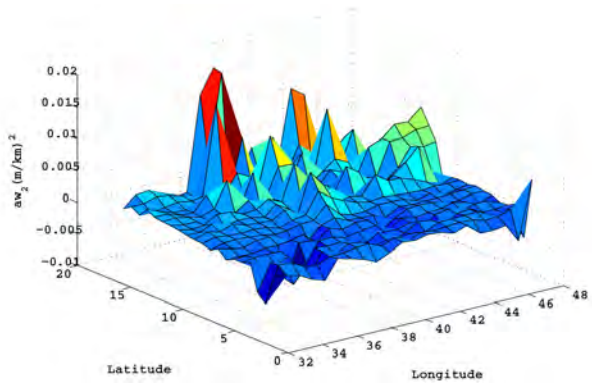

Figure 6.11: The ZWD accelerating rate aw_2 determined from the model during 26-July,2010 - 06-August,2010 in summer season over Ethiopia and its neighbors.

The mean variation of ZTD_{mean} and ZWD_{mean} ranges from 1.8 m to 2.5 m and 0.1 m to 0.22 m, respectively, over the region. The ZTD amplitude (Figures 5.6-5.7), and decreasing and acceleration rate (Figures 5.10-5.11) also change along with the height of each grid. Similarly, the mean annual amplitude variation of ZTD_{amp} and ZWD_{amp} ranges from 0.02 m to 0.1 m over the region. Furthermore, the ZTD_{amp} and the average ZTD_{mean} at average height h_o have similar trend.

6.2.2 The Temporal and Spatial Characteristics of the Model Coefficient

The results in Figures 6.12 - 6.15 illustrate the zenith total and wet delay time series of the temporal and spatial variation of the decreasing rate and the acceleration rate over Ethiopia and its neighbors for some selected location. The decreasing rate a_1 and acceleration a_2 of ZTD, and decreasing rate a_{w1} and acceleration a_{w2} of ZWD are fitted at a 6-hour interval using EAR-Interim pressure level data for each grid point for year 2010. As shown the variation of decreasing and accelerating rate coefficient were occurred due to daily and seasonal change of moisture field.

In Figures 6.16 - 6.17, we also examine the correlation coefficient a_1 and a_2 for ZTDs, and a_{w1} and a_{w2} for ZWDs. The results shown here the correlation coefficient is between 0 and 0.5 for a_1, 0.5 and 1 for a_2, -0.05 and 0.05 for a_{w1}, and -0.1 and 0.1 for

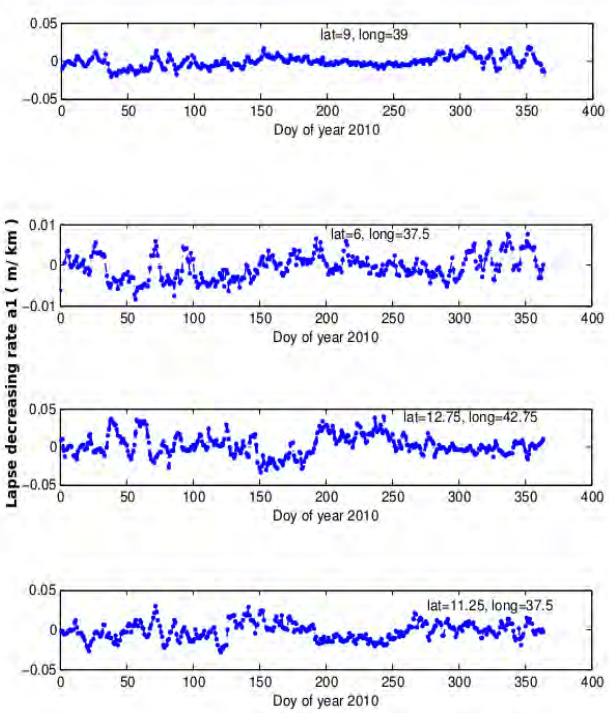

Figure 6.12: ZTD time series of the decreasing rate a_1 on some grid points shownin the legend.

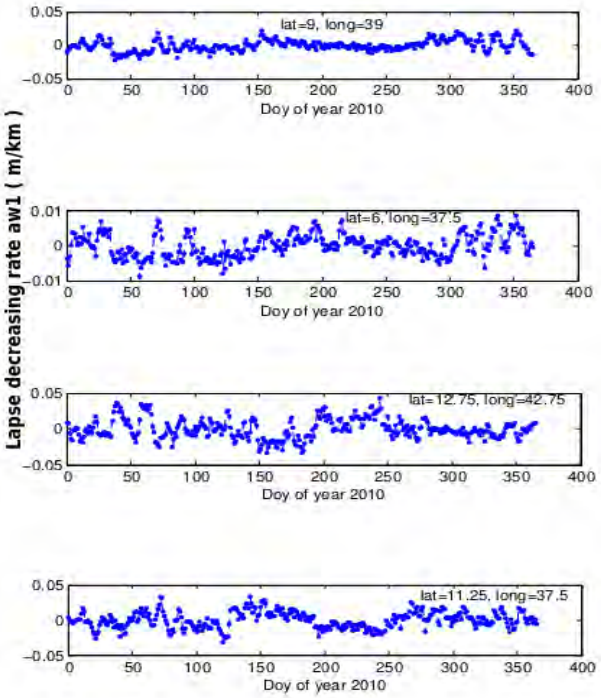

Figure 6.13: ZWD time series of the decreasing rate aw_1 some grid points shown in the legend.

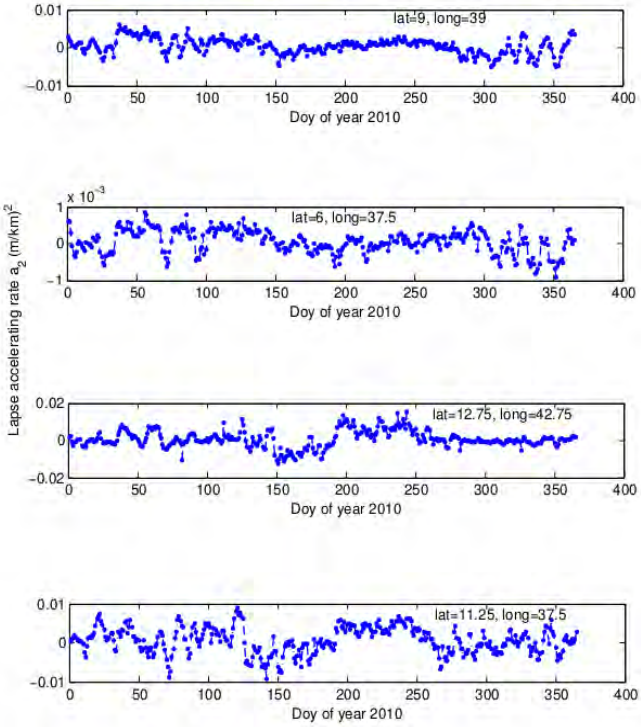

Figure 6.14: ZTD time series of the acceleration rate a_2 some grid points shown in the legend.

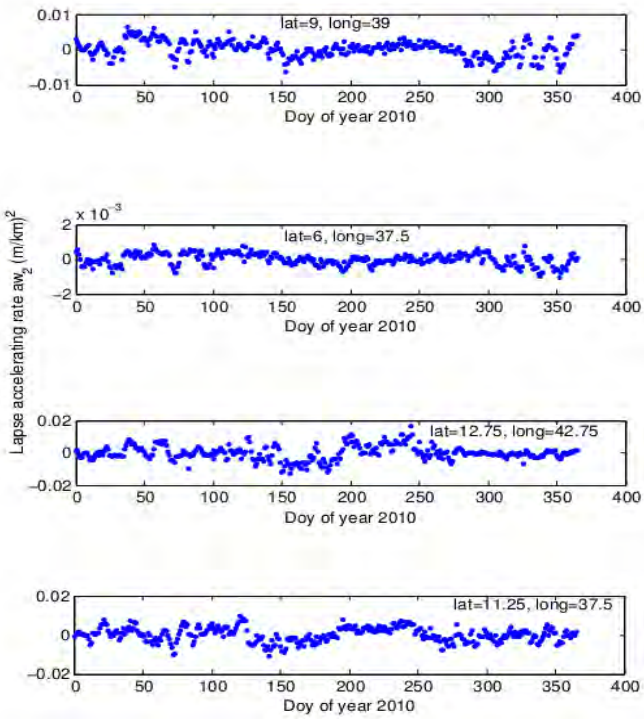

Figure 6.15: ZWD time series of the acceleration rate aw_2 some grid points shown in the legend.

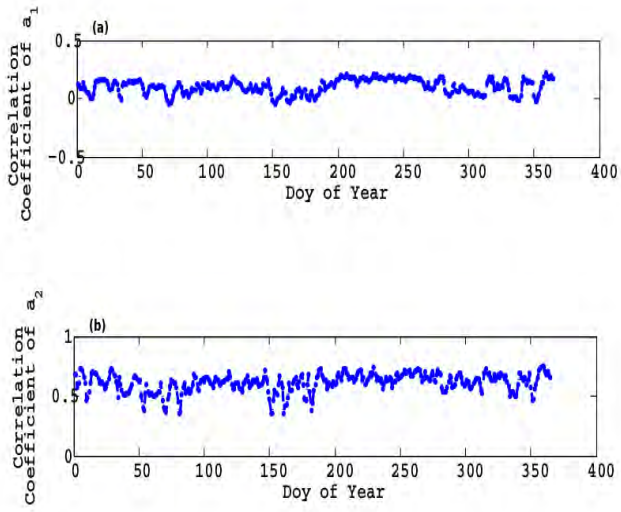

Figure 6.16: ZTD correlation coefficient of the decreasing rate a_1 (a) and acceleration rate a_2 (b) in 2010.

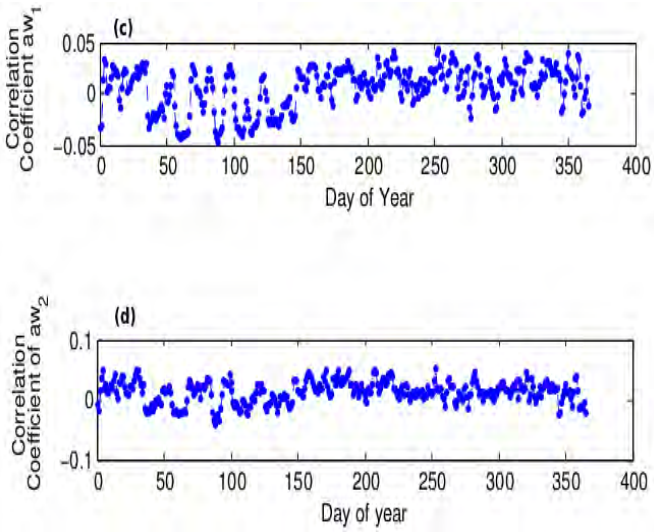

Figure 6.17: ZWD correlation coefficient of the decreasing rate aw_1 (a) and acceleration rate aw_2 (b) in 2010.

a_{w2}, which indicate that there is daily and seasonal change of both the decreasing rate and accelerating rates.

6.3 Validation of the Model precision

In order to verify if the model implementation is truly realistic, a validation process is very important. The validation of the model zenith total delay, zenith wet delay and precipitable water values are performed based on GPS measurements. The GPS data were processed from 2007 to 2011 to determine zenith total delay, zenith wet delays and precipitable water using methods described in Section 6.1. The model zenith total delay (model ZTD), the zenith wet delay (model ZWD) and precipitable water (model derived PW) and its coefficients are interpolated to GPS station by using Shepard interpolation in the nearest grid points.

6.3.1 Validation of Zenith Total Delays

The six stations were used for validation of zenith total delays. Stations are Addis Ababa, Arba Minch, Asab, Bahr Dar, Nazerete and Robe. The forest green sequence represents

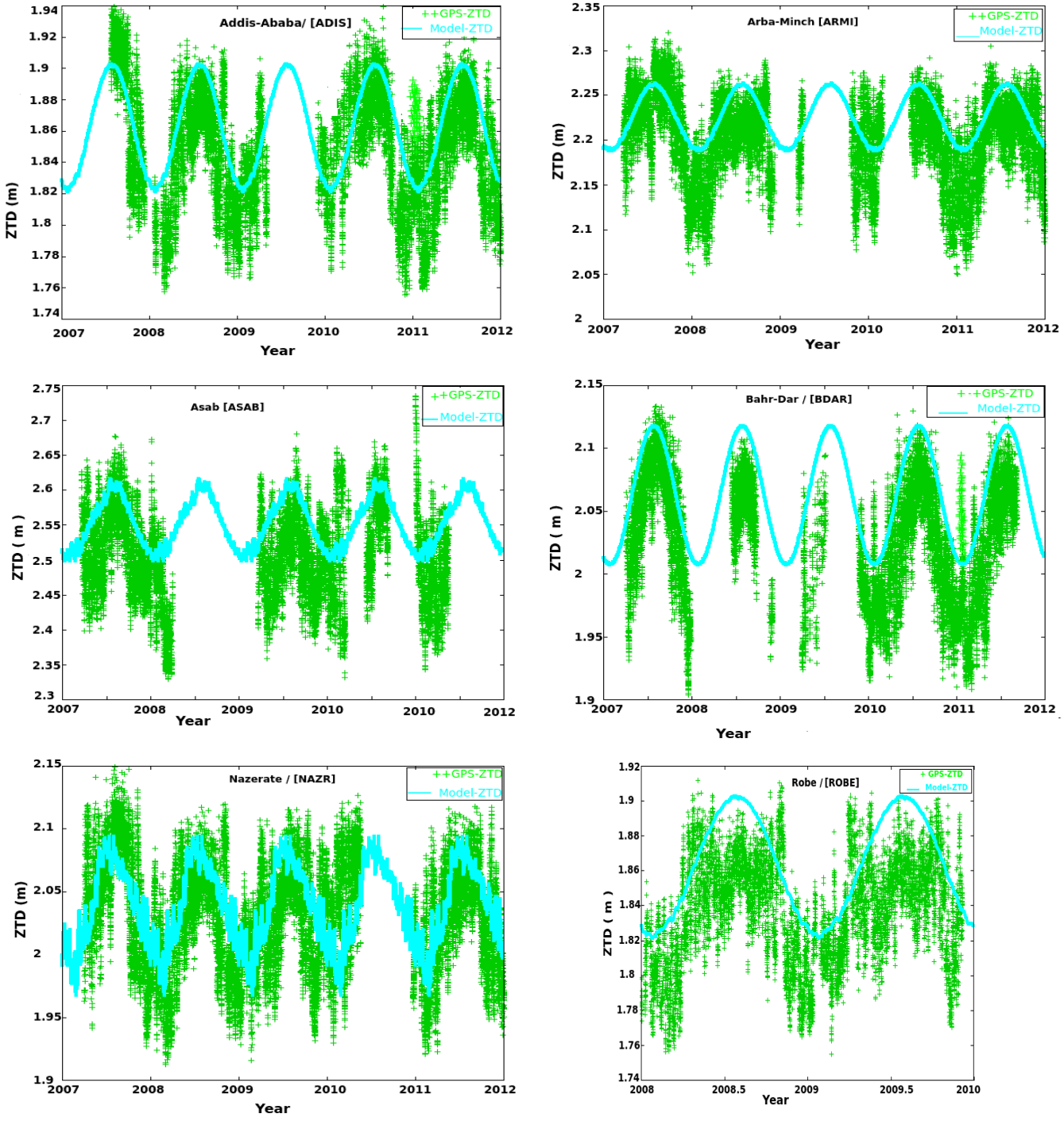

Figure 6.18: Comparison ZTD time series at six GPS station with model and GPS measured ZTD.

the zenith total delays (ZTDs) from GPS measurements and the aqua line represents zenith total delays from model measurements. For all station, as shown in Figure 6.18, the model provides a better fit (good agreement) to the GPS measurements, especially with superior performance in summer season than in winter season. This is because the model decreasing and accelerating rate coefficients accounts for daily and seasonal variations.

In Bahr Dar and Robe station the model overestimates the signal delays while in Addis Ababa, Arba Minch, Asab and Nazerete the model tends to be near the middle of the spread of GPS measurement of tropospheric zenith delays. However, the mean values match the GPS measurement value for all stations. Figure 6.19-6.20 show the four different days of ZTD hourly variation in year 2010 for Addis Ababa and Arba Minch, stations determined using the model interpolation approach and GPS measurements. On one of the day during dry season (date 25-Jan-2010) and wet season (date 25-Oct-2010) the model overestimates the delays for all hours. However, in spring season (date 20-Mar-2010) the model underestimates delay, but closer between 16 and 18 hours (UT). On the other hand, the model ZTDs is much closer to GPS measurement in summer season (date 31-July-2010).

Figure 6.21, shows the day of yearly ZTDs bias during 2007-2011 over Addis Ababa, Arba Minch, Bahr Dar and Nazerete GPS stations. The bias between the model derived and GPS measurement zenith total delays has a mean that varies in the range of -6.34 cm to 3.16 cm over the years. The maximum bias for Addis Ababa, Arba Minch, Bahr Dar and Nazerete GPS stations are 7.899, -13.5760, 16.740 and 17.744 cm, respectively at the beginning of 2011. In general, the bias has more of a symmetric shape through the study period.

Figure 6.22 shows that daily average ZTDs bias for the period 2007-2011 at Addis Ababa, Arba Minch, Bahr Dar and Nazerete GPS stations. All The GPS stations exhibit negative bias for most of the Observation periods except for Nazerete GPS station which exhibits negative bias in the summer and mixed bias during the rest of the year.

Figure 6.23 (a)-(b) show average monthly ZTDs bias for GPS station at Arba Minch and Nazerete between 2007-2011. The maximum bias at Arba Minch and Nazerete are

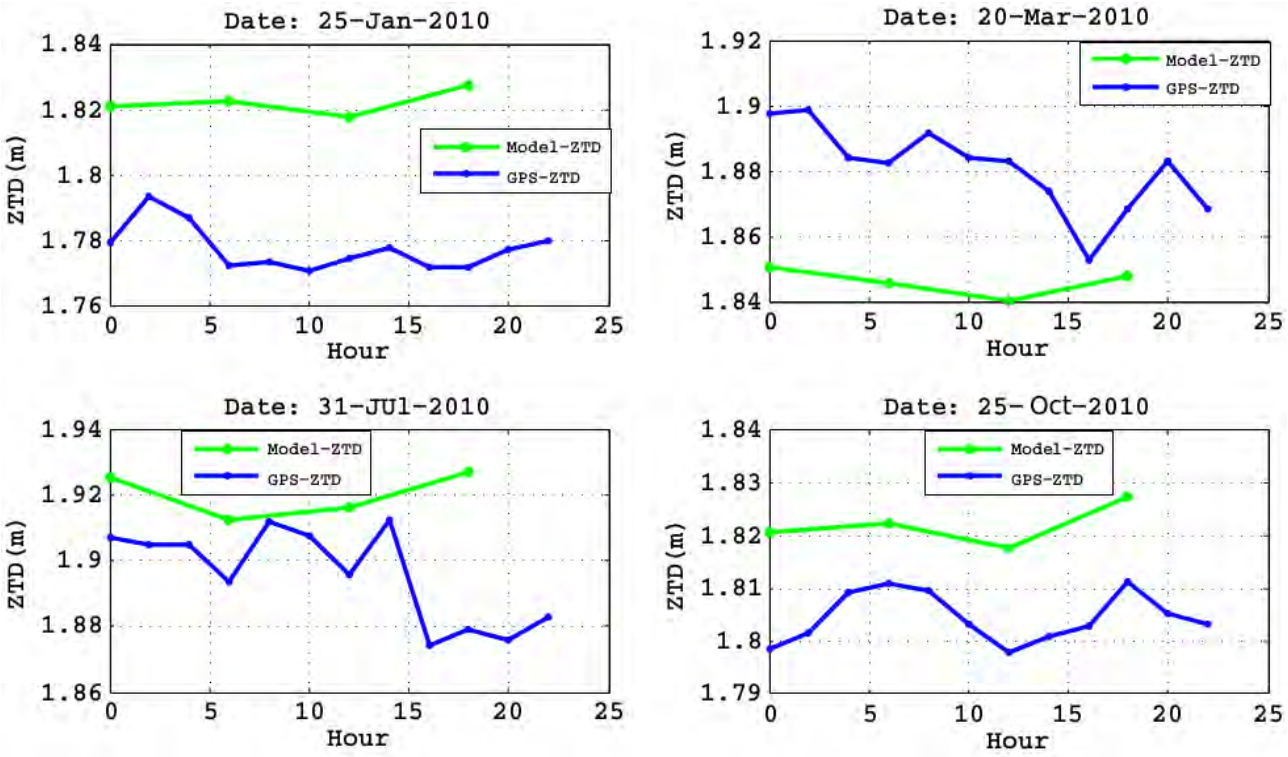

Figure 6.19: Hourly comparison of zenith tropospheric delays estimated from model and the final values produced by GPS for the station Addis Ababa (ADIS), Ethiopia.

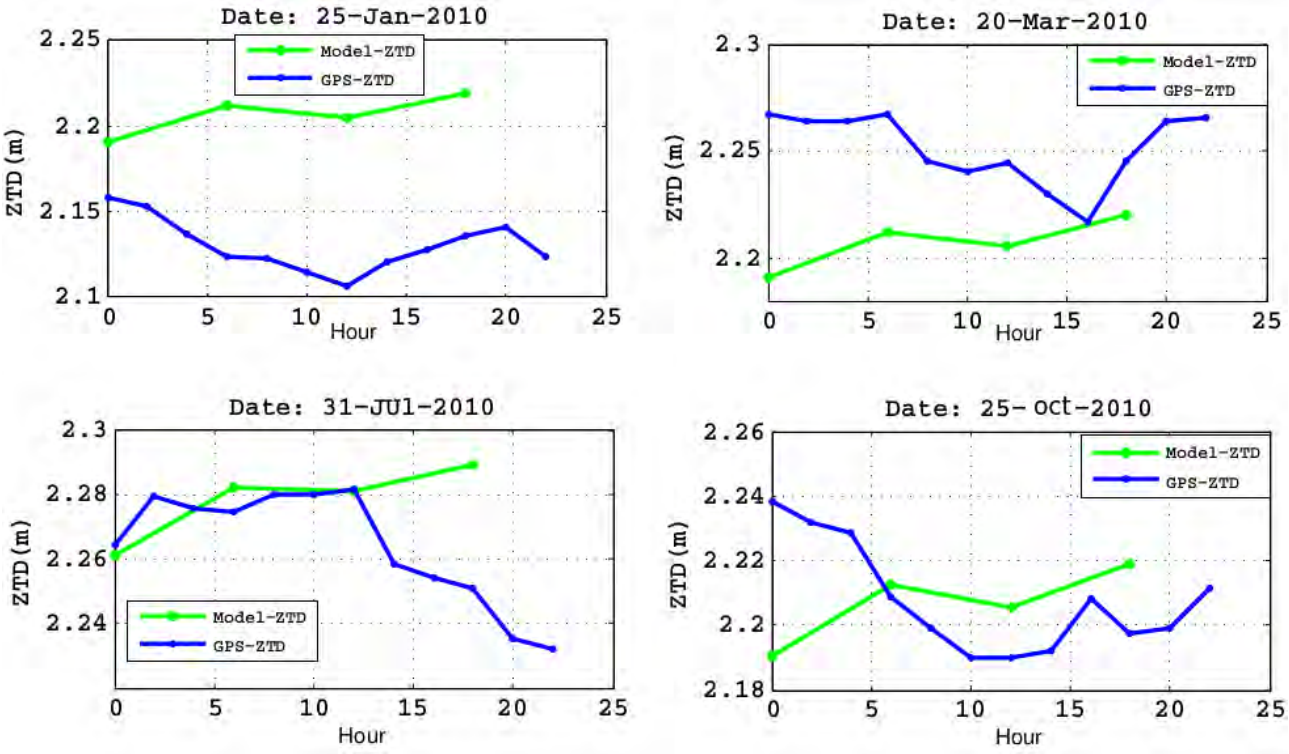

Figure 6.20: Hourly comparison of zenith tropospheric delays estimated from model and the final values produced by GPS for the station Arba Minch (ARMI), Ethiopia.

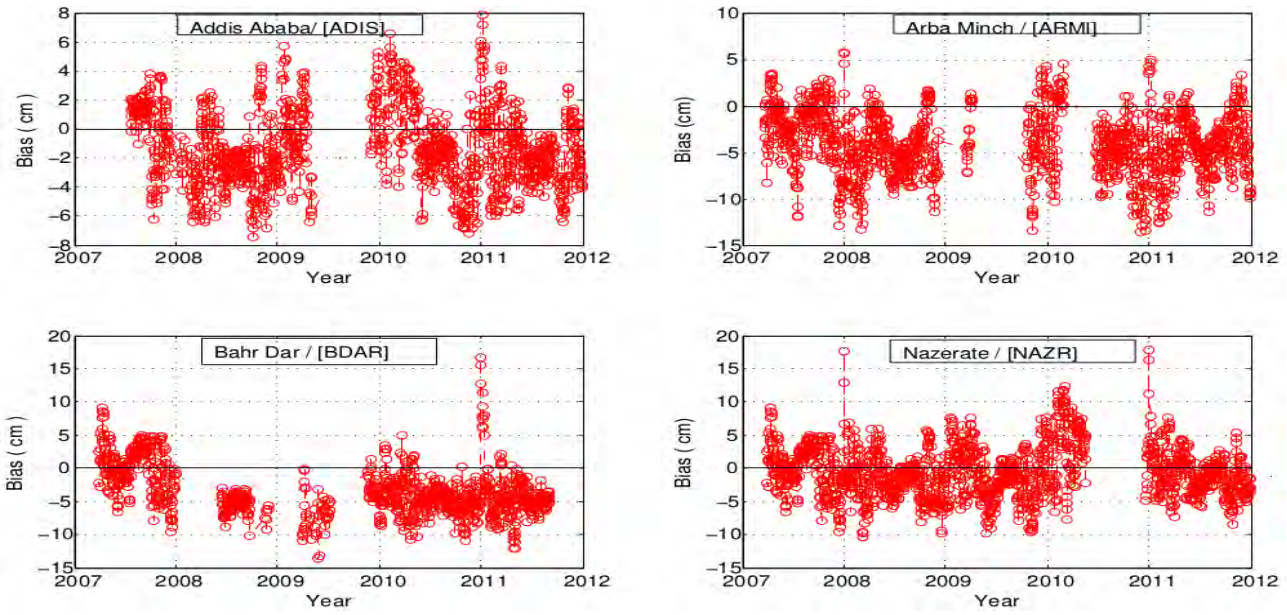

Figure 6.21: Difference in ZTD with the model derived estimates and GPS measurement between the day of year 2007 - 2011 at the GPS stations of Addis Ababa (ADIS), Arba Minch (ARMI), Bahr Dar (BDAR) and Nazerete (NAZR), Ethiopia

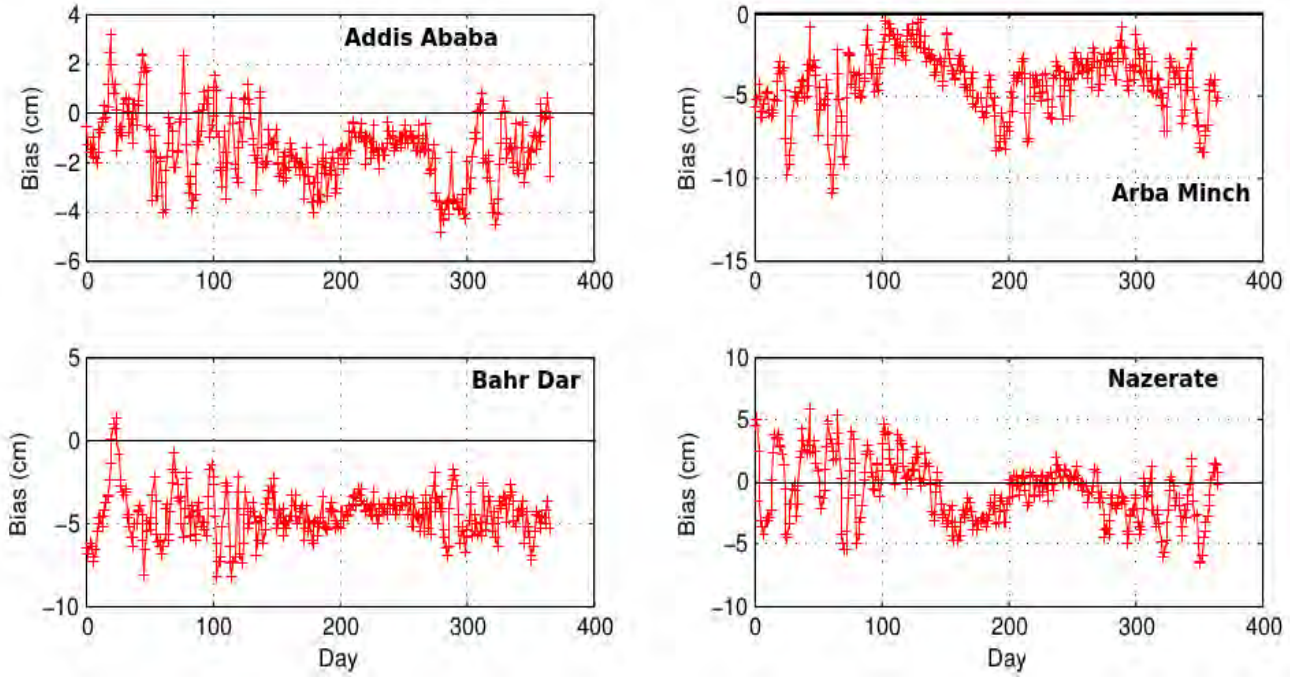

Figure 6.22: Daily avarege ZTDs bias with the model estimates and GPS measurement products between the ear 2007 - 2011 at the GPS stations Arba Minch (ARMI) and Nazerete (NAZR), Ethiopia

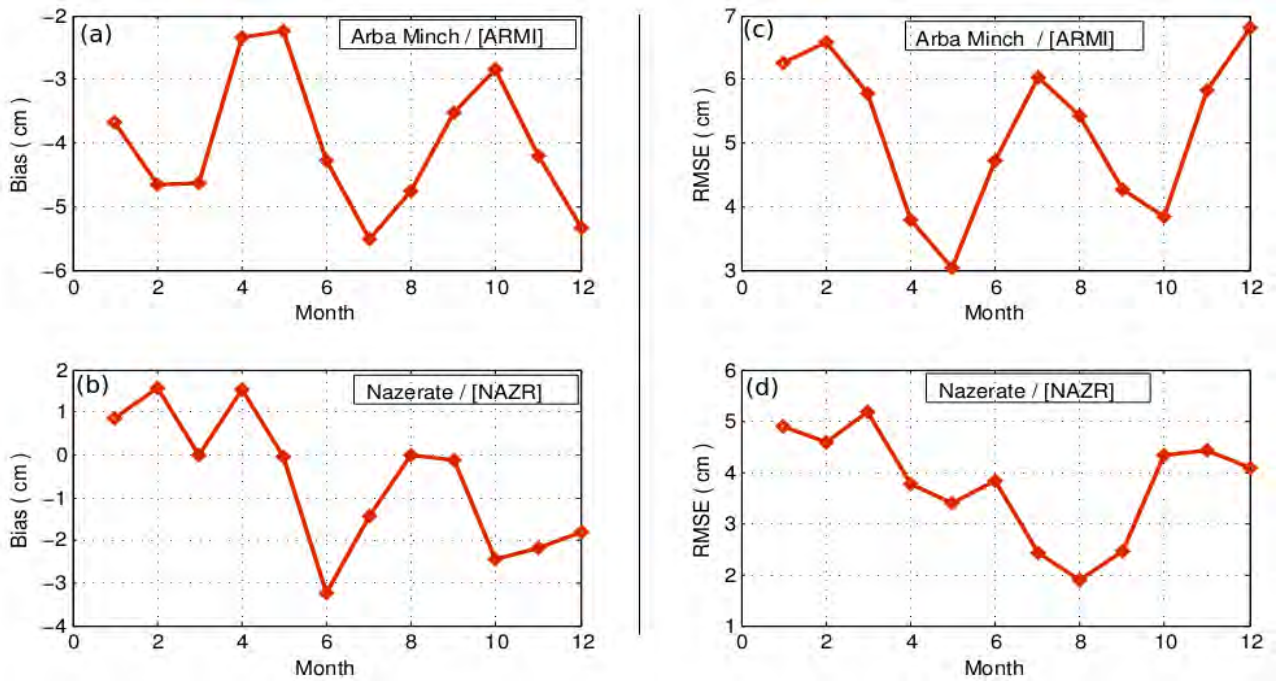

Figure 6.23: Monthly avarege bias in ZTDs with the model-derived estimates and GPS measurement products between the ear 2007 - 2011 at the GPS stations Arba Minch (ARMI) and Nazerete (NAZR), Ethiopia

-5.503 cm in July and -3.2255 cm in June, respectively, which indicate the model ZTDs are biased towards wet for both stations. Tables 6.2 shows that for all the six stations, the biases of the model are in the range of -7.1059 cm to 1.5755 cm, with the mean value of -3.9963 cm. The maximum bias is at ASAB (ASAB is the least deep altitude or low land areas and near to sea) in June. In general, all of the stations have average monthly minimum and positive bias at winter season, and maximum and negative bias at summer season, which reflects the model ZTDs are biased towards wet. Figure 6.22 (c)-(d) show average monthly ZTDs RMSE for Arba Minch and Nazerete from 2007 to 2011. The maximum RMSEs at Arba Minch and Nazerete are 6.8129 in December and 5.1632 in March, respectively. Likewise, from Table 5.3, we can see that the RMSEs of model ZTDs are in the range of 1.8833 cm to 9.5640 cm, with the mean value of 4.9265 cm. The maximum is 9.5640 cm at ASAB station in March and the minimum bias of 1.8833 cm is at Nazerete station in August.

Figures 5.23-6.24 illustrate the hourly difference between zenith total delays (ZTD) for

Table 6.2: Average monthly bias Zenith total delays (ZTDs) of the model with GPS between year 2007-2011 at each station, with the unit of cm.

Site	Month											
	Jan	Feb	Mar	Apr	May	Jun	Jul	Aug	Sep	Oct	Nov	Dec
ADIS	0.0075	-0.5165	-1.0790	-0.2547	-1.4910	-2.3245	-1.2882	-1.2262	-1.2610	-3.7348	-1.5465	-1.8175
ARMI	-3.6659	-4.6611	-4.6352	-2.3439	-2.2368	-4.2879	-5.5030	-4.7470	-3.5142	-2.8406	-4.1928	-5.3275
ASAB	-0.5569	-3.4644	-5.9285	-5.5647	-7.1059	-8.2219	-4.4705	-2.8105	-5.0536	-7.0129	-5.3038	-3.1118
BDAR	-1.0292	-5.0432	-4.1155	-5.0196	-4.8563	-5.0081	-4.6456	-3.9319	-4.2855	-4.3086	-4.3793	-4.7996
NAZR	0.8482	1.5755	0.0034	1.5386	-0.0417	-3.2255	-1.4297	0.0096	-0.1327	-2.4265	-2.1638	-1.8124
ROBE	0.1780	-1.8646	-2.5082	0.1135	-2.0055	-3.9798	-3.8429	-3.1978	-2.0522	-1.4941	-1.5196	-2.6622

Table 6.3: Average monthly RMSE Zenith total delays (ZTDs) of the model with GPS between year 2007-2011 at each station, with the unit of cm.

Site	Months											
	Jan	Feb	Mar	Apr	May	Jun	Jul	Aug	Sep	Oct	Nov	Dec
ADIS	3.5405	3.1150	3.1782	2.8360	2.7722	2.7900	2.3273	2.0817	2.2875	4.4950	3.2657	2.4305
ARMI	6.2581	6.5882	5.7816	3.7918	3.0270	4.7316	6.0416	5.4360	4.2608	3.8408	5.8205	6.8129
ASAB	6.0232	7.4113	9.5640	7.9072	8.3820	8.8849	5.7226	4.2880	6.2338	8.0624	7.2516	4.5065
BDAR	5.9146	5.4714	5.2223	5.9560	5.7998	5.3295	4.9062	4.2339	4.6932	4.9242	5.2276	5.2285
NAZR	4.8781	4.5705	5.1632	3.7552	3.3859	3.8338	2.4117	1.8833	2.4681	4.3232	4.4165	4.0867
ROBE	4.4019	2.6414	3.3881	2.4304	2.7384	4.3784	4.2394	3.8320	2.8792	2.8837	3.7007	3.3633

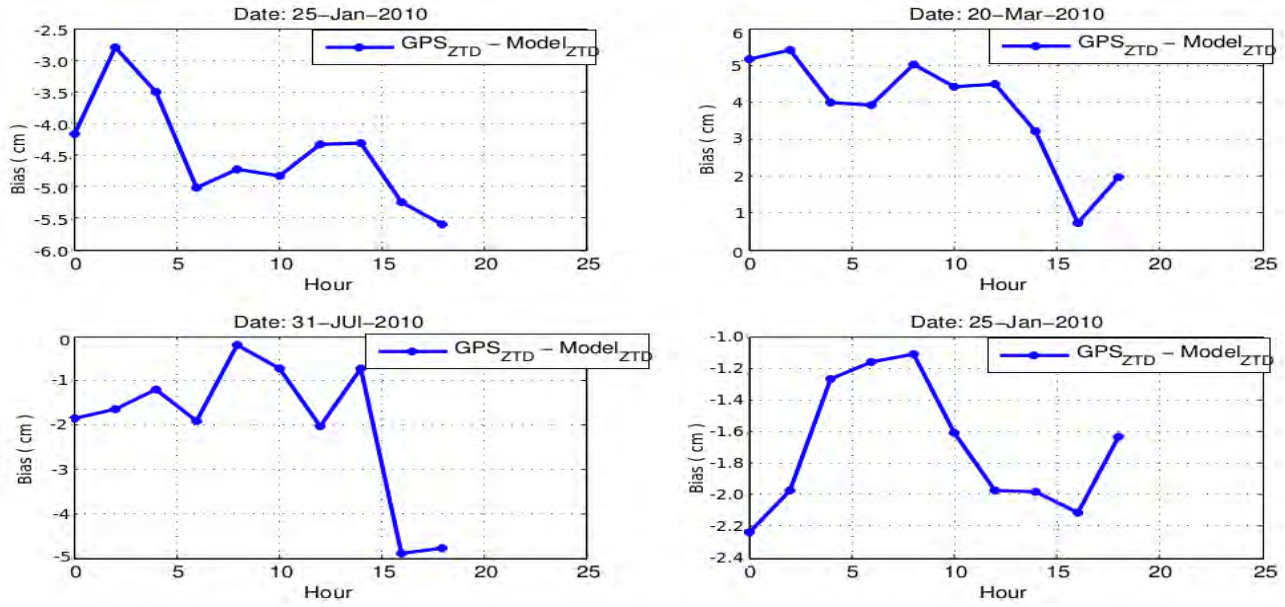

Figure 6.24: Hourly difference in ZTDs between the model estimates and GPS products at the GPS station Addis Ababa (ADIS), Ethiopia.

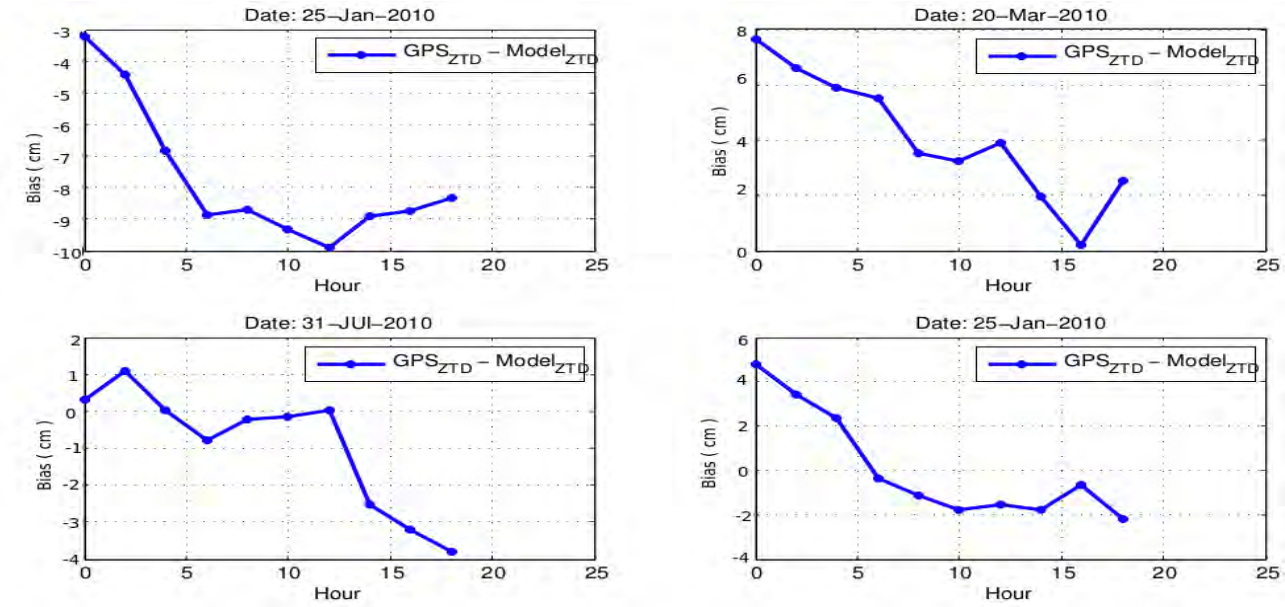

Figure 6.25: Hourly difference in ZTDs between the model derived estimates and GPS products at the GPS station Arba Minch (ARMI), Ethiopia.

Table 6.4: Mean, standard deviation and RMS of the difference between GPS derived and Model derived based zenith total delays (ZTDs).

Site Name	No. Test	Date	Statistics [GPS_ZTD - Model_ZTD]				
			Min(cm)	Max(cm)	Mean(cm)	std(cm)	RMS(cm)
ADIS	1	January 25th	-2.80500	-5.59100	-4.45410	0.78731	0.78731
	2	March 20th	0.72500	5.41300	3.83840	1.41452	1.41452
	3	July 31th	-0.19133	-4.90500	-1.99150	1.53277	1.53277
	4	October 27th	-1.1133	-2.23800	-1.70710	0.41202	0.35682
ARMI	1	January 25th	-3.22800	-9.87900	-7.71950	2.10380	2.10380
	2	March 20th	0.20867	7.65400	4.10100	2.17595	2.17595
	3	July 31th	1.10933	-3.81300	-0.91840	1.57470	1.57470
	4	October 27th	-2.19800	4.76200	0.11050	2.47739	2.14548

selected day (hourly values) determined using the model estimate and GPS. The mean difference between the model estimate and GPS based zenith total delays varies in the range of -5.5910 cm (January 25^{th}) and -0.19133 cm (July 31^{th}) for Addis Ababa; and -9.8790 cm (January 25^{th}) and 0.2086 cm (March 31^{th}) for Arba Minch. For the selected winter day (January 25^{th}) and Autumn season (October 25^{th}) the bias is negative. However, in spring season (March 20^{th}) and in summer season (July 31^{th}) the bias is positive except at 16 and 18 hours (UT). The minimum RMSE were occurred on January 25 for both station. A summary of yearly biases, monthly average biases and RMSEs, and hourly biases and RMSEs statistics for the selected site are given in Table 5.2, Table 6.3 and Table 6.4.

6.3.2 Validation of Zenith Wet Delays (ZWD)

Figure 6.26 shows the comparison of GPS derived ZWD and model estimate for the eight station. The green sequence represents ZWD time series measured by GPS and the yellow

one represents the ZWD time series estimatedby model. As clearly shown in Figure 6.26 the model zenith wet delays provides a more better fit to the GPS measurement for all season compared with the model zenith total delays (Figure 6.18). This reflects the model ZTD is hydrostatics (dry) biased. For instance, in Figure 6.25 at Bahr Dar and Robe the model zenith wet delays tends to be near the middle of the spread of GPS measurement, but in Figure 6.18 the model zenith total delays are slightly overestimated.

Figure 6.27 illustrates the bias of zenith wet delays between 2007-2011 at different station. As seen, the bias has a mean that varies in the range between -3.0255 cm to 1.5984 cm. The maximum bias is 22.6180 year 2011 at station Asab, but not in Asab there is also maximum bias for the selected stations in year 2011. For all case of stations, the bias is almost below zero and similar to bias ZTDs (Figure 6.21) are symmetric.

Figure 5.28 shows daily average of difference of ZWDs of the model estimates and GPS measurement for 2007-2011 period at Addis Ababa, Arba Minch, Bahr Dar and Nazerete GPS station. The daily mean bias varies in the range -3.42 cm to 0.584 cm. The basic reason for the bias linked with the model wet decreasing rate a_{1w} and accelerating rate a_{2w}.

Figure 6.29 and Table 6.5 shows that an average monthly ZWDs bias and RMSE . Here both the bias and RMSE variations are very large. The reason for this is that water vapor is highly variable with time and space, and the wet delays represent the real atmosphere at a particular time only if tropospheric parameters are estimated at that given time accurately. A maximum average monthly bias and RMSE were occurred at Asab -7.5071 and 8.2459; and Robe -8.6842 and 8.8901 in June, respectively. Similarly, all stations get maximum bias and RMSE in June, July and August months, which is rainy season in Ethiopia.

In general, these figures and tables clearly show that the bias and RMSEs during the summer months are larger than those of the winter months. The variability of ZTDs , especially during summer season has come from the variability in ZWD. These characteristics are correlated with the complex and variable summer weather in Ethiopia and its neighbors.

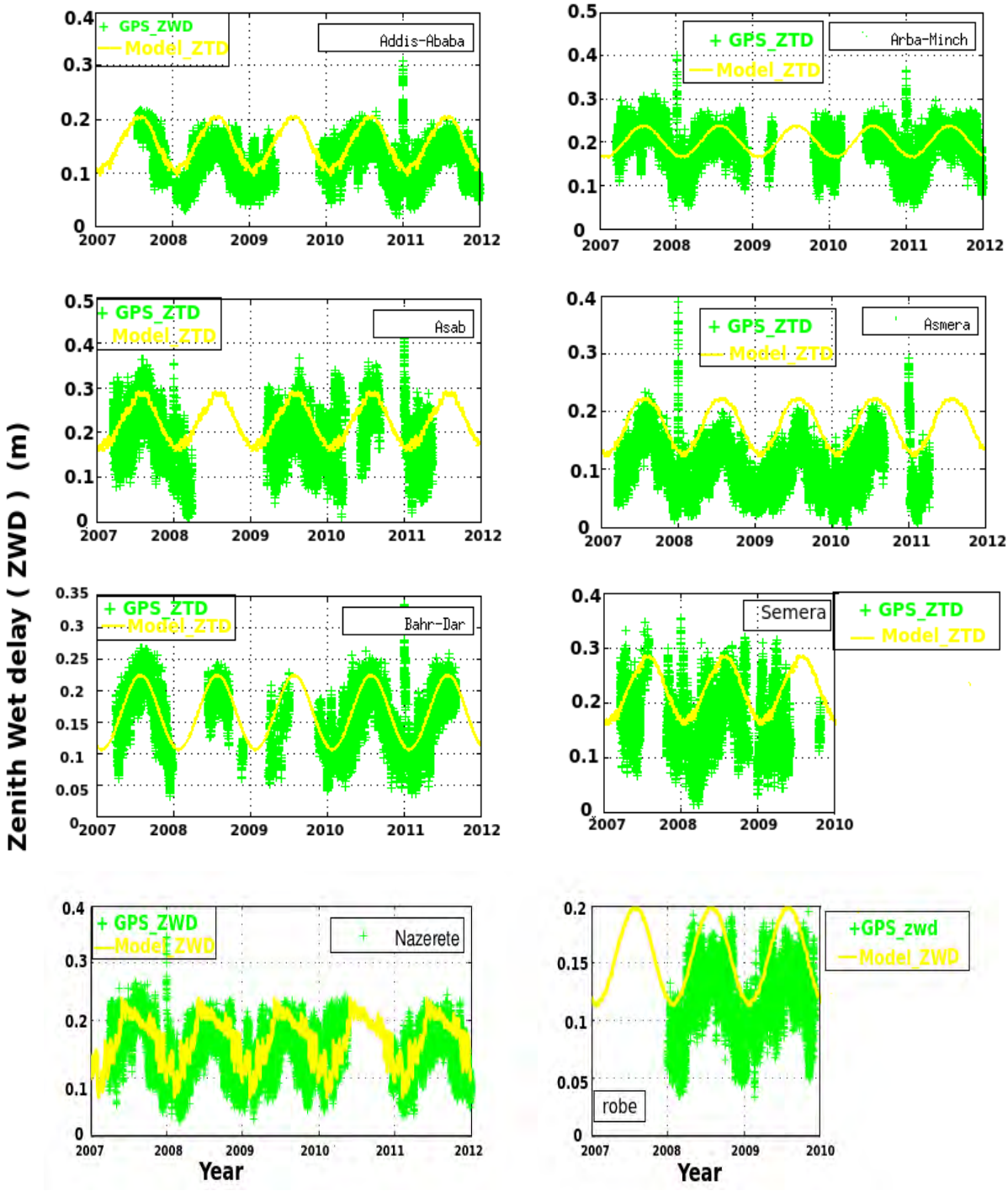

Figure 6.26: Time series comparison of the zenith wet delay (ZWD) with the model estimates and GPS measurement products between the day of year 2007-2011 at the GPS stations of Addis Ababa, Arba Minch, Asab, Asmera, Bahr Dar, Semera, Nazerete and Robe, Ethiopia.

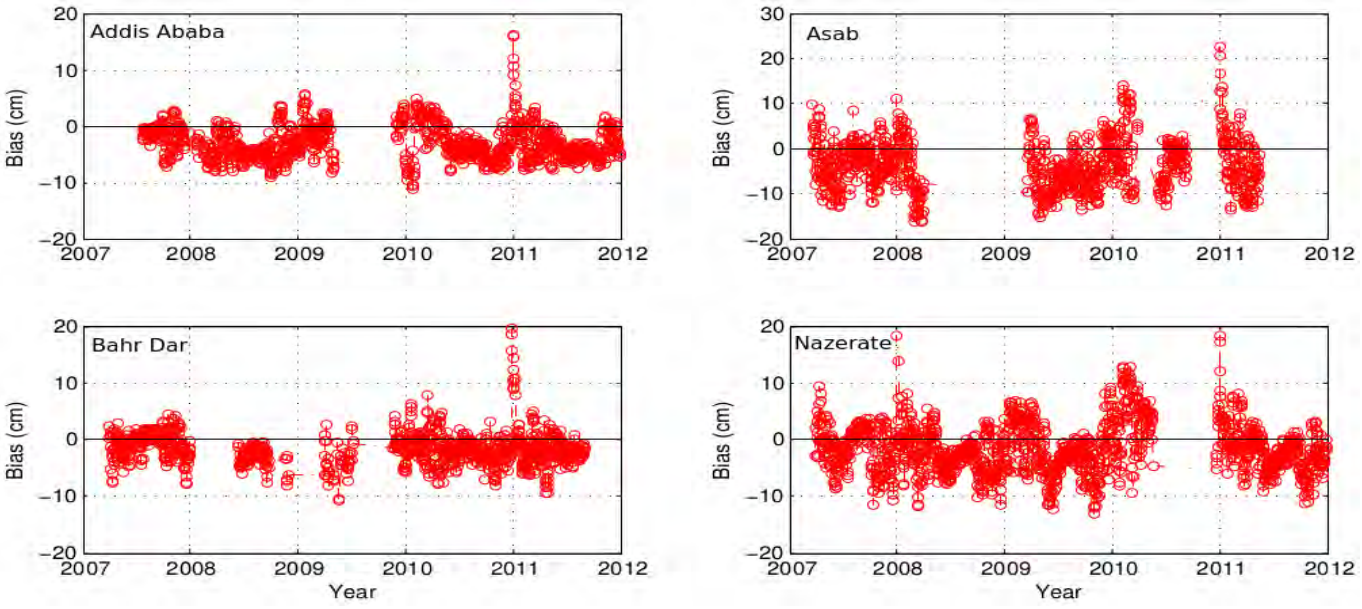

Figure 6.27: Difference in ZWD with the model-derived estimates and GPS measurement between the day of year 2007-2011 at the GPS stations ofAddis Ababa, Asab, Bahr Dar and Nazerete, Ethiopia

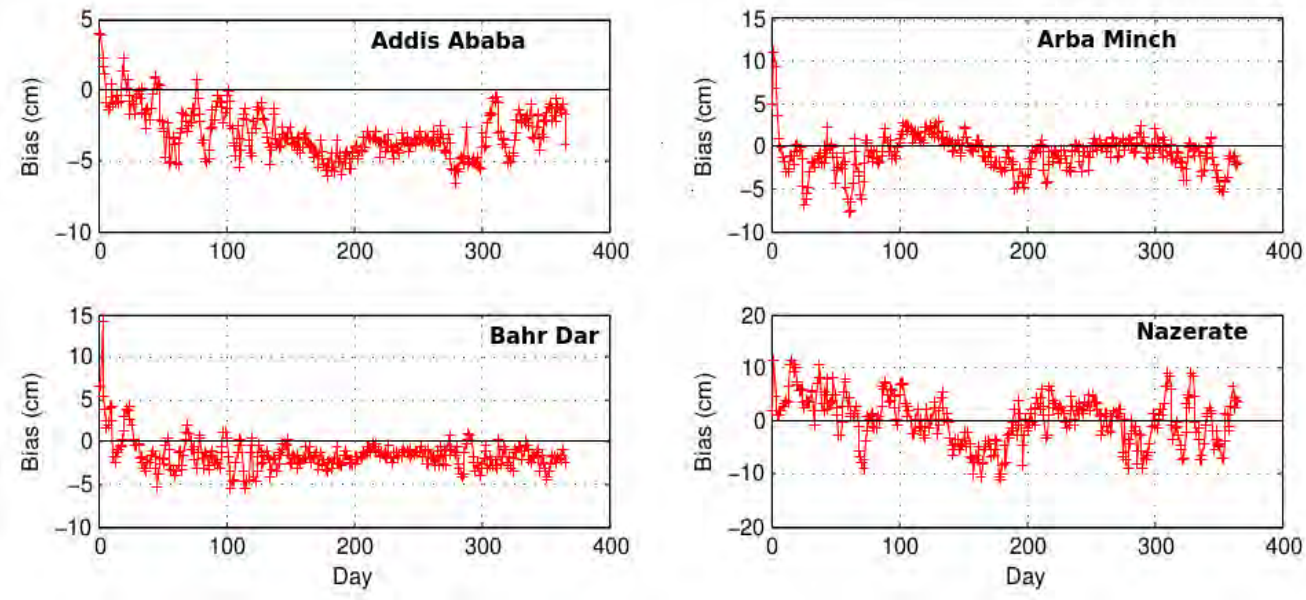

Figure 6.28: Daily avarege bias in ZTDs with the model-derived estimates and GPS measurement products between the year 2007 - 2011 at the GPS stations Addis Ababa, Arba Minch, Bahr Dar and Nazerete, Ethiopia

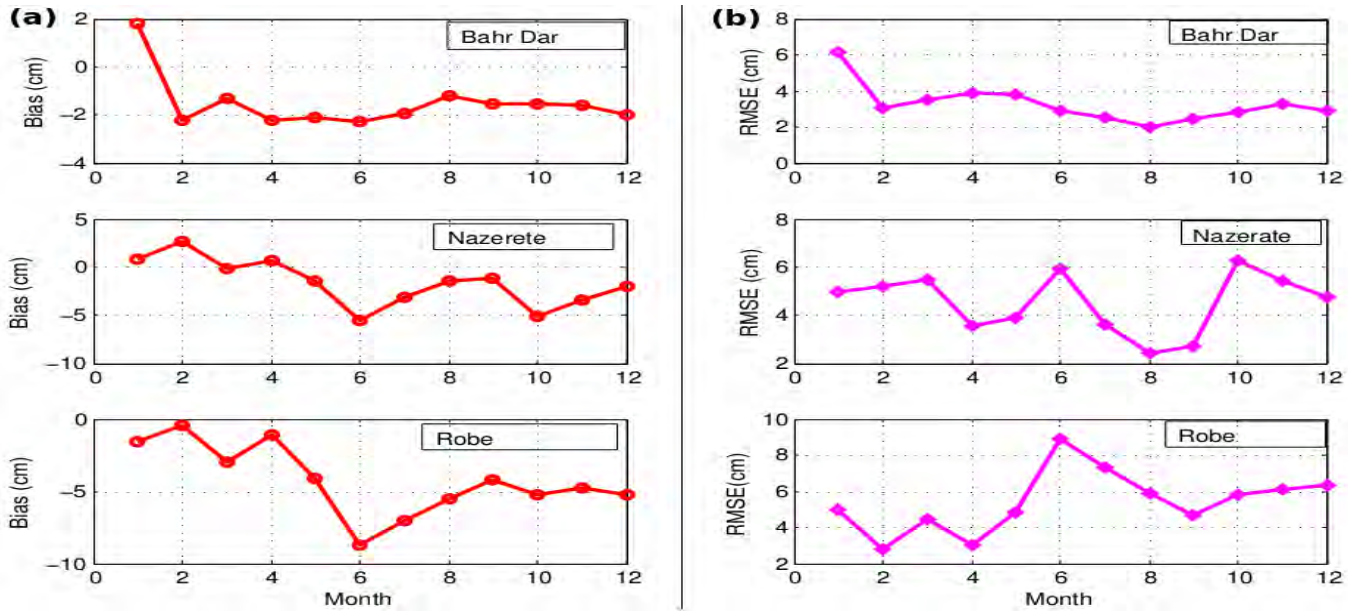

Figure 6.29: Monthly avarege (a) difference (b) RMSEs , in ZWD with the model-derived estimates and GPS measurement products between the day of year 2007-2011 at the GPS stations ofAddis Ababa, Arba Minch, Bahr Dar and Nazerete, Ethiopia

Table 6.5: Average monthly bias and RMSE between 2007-2011 at each station for model derived with GPS derived based zenith wet delays (ZWDs), where the unit is cm.

Site		Month											
		Jan	Feb	Mar	Apr	May	Jun	Jul	Aug	Sept	Oct	Nov	Dec
ADIS	Bias	-1.3640	-1.7941	-2.5477	-2.0691	-2.9503	-4.3737	-4.4374	-3.8020	-3.5251	-4.6705	-2.6334	-2.1042
	rmse	5.5776	3.7673	3.8915	3.4213	3.7613	4.6391	4.6682	4.1896	4.0678	5.3540	4.0489	3.1612
ARMI	Bias	-0.5442	-1.5619	-1.4922	0.8728	1.0334	-0.9693	-2.1540	-1.3943	-0.1941	0.4213	-0.9999	-2.1968
	rmse	5.1571	4.9079	3.7721	3.1228	2.2802	2.2158	3.2997	3.0032	2.4281	2.6221	4.1652	4.7844
ASAB	Bias	1.1244	-1.8658	-4.4832	-4.4290	-6.1710	-7.5071	-3.7860	-2.0695	-4.1473	-6.0181	-3.9479	-1.5185
	rmse	6.1582	6.8641	8.0708	7.1704	7.5873	8.2459	5.2187	3.8770	5.5240	7.1981	6.3629	3.6103
BDAR	Bias	1.8180	-2.2207	-1.3102	-2.2437	-2.1115	-2.2937	-1.9399	-1.2161	-1.5516	-1.5425	-1.5853	-1.9936
	rmse	6.1432	3.0710	3.4734	3.9158	3.8106	2.9309	2.5032	1.9945	2.4715	2.8449	3.2737	2.8749
NAZR	Bias	0.8594	2.6084	-0.1940	0.6247	-1.4774	-5.5044	-3.1578	-1.4385	-1.2191	-5.0953	-3.4259	-1.9899
	rmse	4.9798	5.2246	5.4945	3.5399	3.9196	5.9265	3.6277	2.3965	2.7097	6.2462	5.4147	4.7655
ROBE	Bias	-1.5615	-0.4406	-3.0074	-1.0784	-4.1092	-8.6842	-7.0305	-5.5146	-4.1912	-5.2103	-4.7934	-5.2600
	rmse	5.0140	2.8127	4.4424	3.0110	4.8215	8.8901	7.3044	5.8983	4.6537	5.7974	6.1507	6.3247

6.3.3 Validation of Precipitable Water (PW)

Precipitable water vapor (PW) is estimated from model based on zenith wet delays ZWDs. Figure 6.30 describes the time series of PW which is obtained form GPS measurement and model. The green sequence represents the precipitable water (PW) from GPS measurements and the yellow line represents PW from model. The GPS measured PW time series are computed using software (GAMIT) described in previous chapter, and the model PW time series is derived form model zenith wet delays (ZWDs). As shown in the figures, the PW time series has the same feature as ZTDs and ZWDs. In case of Asmera and Semera, the model derived PW is overestimated, probably due to interpolation errors. However, in the other stations the model derived PW fit well (good agreement) to the GPS PW measurement.

Figure 6.31 illustrate the the yearly PW bias in PW of the model derived estimates with respect GPS measurement during 2007-2011 at Addis Ababa, Asab, Bahr Dar and Nazerete GPS stations. The bias is very small and almost below zero for all stations. Moreover, PW bias has a mean that varies in the range of -1.52 cm to 0.584 cm. For all cases the maximum bias of 4 cm occurred in 2011 winter season at Asab station. Similarly, Bahr Dar and Nazerete have maximum PW bias of 3.12cm.

Figure 6.32 shows daily avarege PW bias of the model with respect to GPS measurement for 2007-2011 at Addis Ababa, Arba Minch, Bahr Dar and Nazerete GPS stations. Again similar to ZTDs and ZWDs through out the day of year, except winter season, the change of bias is uniform.

In winter season almost all stations have positive daily bias, which indicates dry bias in this season. The average daily PW bias has a mean that varies in the range of -1.12 cm to -0.34 cm. The maximum daily bias is 2.3 (positive) at Bahr Dar station in winter season.

Table 6.6 and Figure 6.33 show monthly average PW bias and RMSEs of the model estimates with respect GPS measurement for 2007-2011 at of Addis Ababa, Arba Minch, Bahr Dar and Nazerete GPS stations. All stations have positive bias in January, except Robe. In summer season (June, July and August) the mean bias is maximum compared

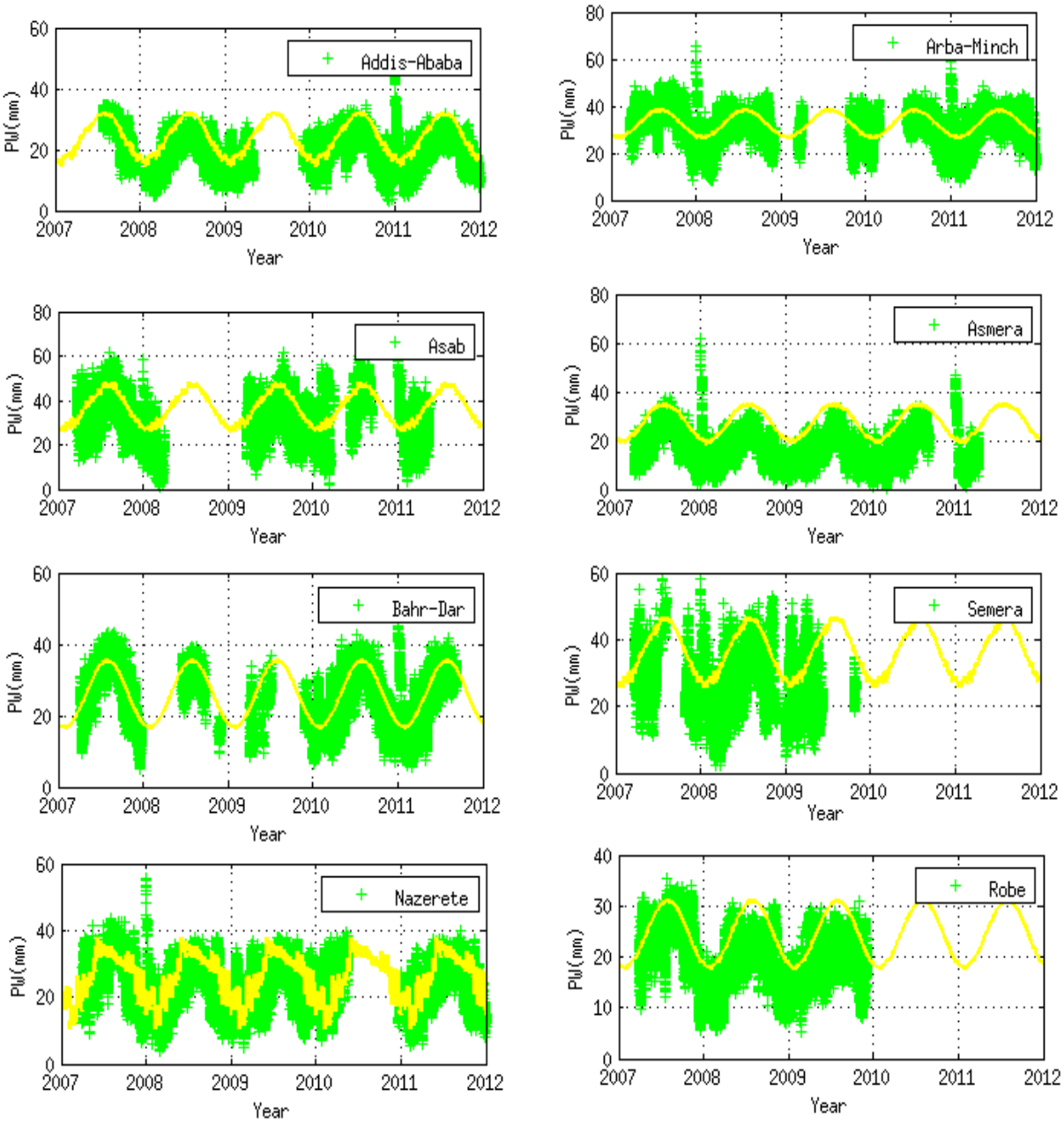

Figure 6.30: Time series comparison of precipitable water (PW) between the model derived and GPS measurement products at the GPS stations of Addis Ababa, Arba Minch, Asab, Asmera, Bahr Dar, Semera, Nazerete and Robe, Ethiopia.

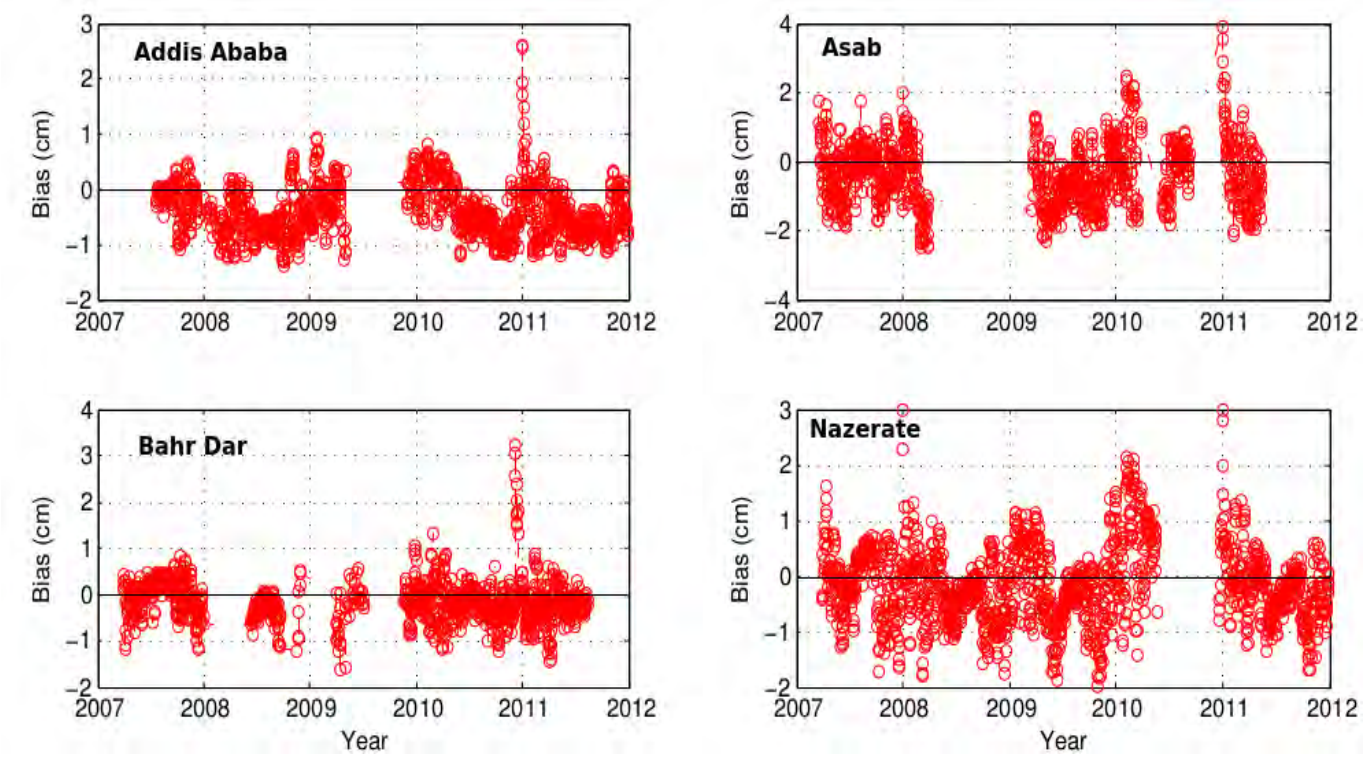

Figure 6.31: Difference in PW with the model-derived estimates and GPS measurement products between the day of year 2007-2011 at the GPS stations of Addis Ababa, Asab, Bahr Dar and Nazerete, Ethiopia

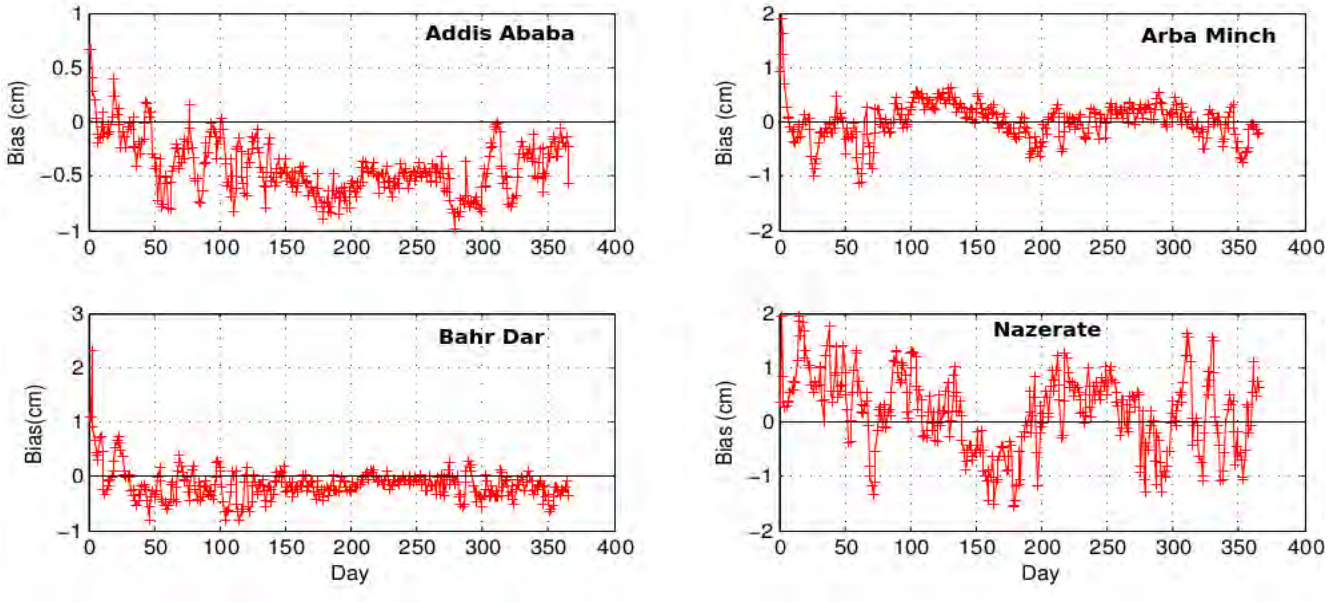

Figure 6.32: Daily avarege bias in PW with the model-derived estimates and GPS measurement products between the year 2007-2011 at the GPS stations Addis Ababa, Arba Minch, Bahr Dar and Nazerete, Ethiopia

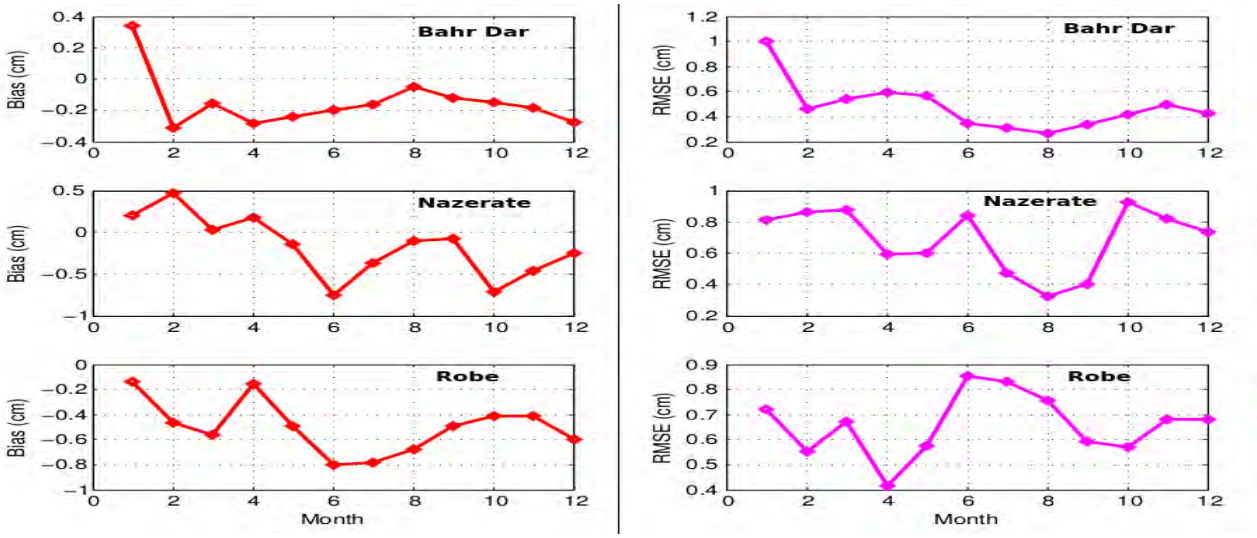

Figure 6.33: Monthly average (a) difference (b) RMSEs , in PW with the model-derived estimates and GPS measurement products between the day of year 2007-2011 at the GPS stations of Addis Ababa, Arba Minch, Bahr Dar and Nazerete, Ethiopia

Table 6.6: Average monthly bias and RMSE between 2007-2011 at each station for model derived with GPS derived based precipitable water (PW), where the unit is cm.

Site		Month											
		Jan	Feb	Mar	Apr	May	Jun	Jul	Aug	Sept	Oct	Nov	Dec
ADIS	Bias	0.0417	-0.2541	-0.3691	-0.2811	-0.3969	-0.6201	-0.6198	-0.5179	-0.4837	-0.6861	-0.3747	-0.3012
	rmse	0.6617	0.5847	0.5966	0.5169	0.5400	0.6676	0.6625	0.5903	0.5835	0.8036	0.6183	0.4815
ARMI	Bias	0.0154	-0.1504	2.5449	0.2581	0.3166	0.0075	-0.1770	0.0405	0.1313	0.5426	0.7106	0.7900
	rmse	0.8334	0.7711	0.3629	0.5164	0.4574	0.3239	0.4460	0.4394	0.4168	0.7445	0.6361	0.5669
ASAB	Bias	0.3354	-0.1509	-0.5664	-0.5229	-0.7821	-0.9590	-0.2991	-0.0077	-0.3907	-0.7504	-0.4530	-0.0829
	rmse	1.0569	1.1028	1.3740	1.0699	1.0744	1.1175	0.6767	0.5514	0.7285	1.0000	0.9424	0.5471
BDAR	Bias	0.3381	-0.3096	-0.1525	-0.2833	-0.2390	-0.1979	-0.1663	-0.0495	-0.1203	-0.1471	-0.1819	-0.2761
	rmse	1.0019	0.4605	0.5402	0.5901	0.5690	0.3429	0.3074	0.2628	0.3366	0.4158	0.4965	0.4214
NAZR	Bias	0.1947	0.4623	0.0286	0.1793	-0.1376	-0.7579	-0.3753	-0.1019	-0.0790	-0.7171	-0.4677	-0.2556
	rmse	0.8111	0.8596	0.8790	0.5896	0.5981	0.8373	0.4739	0.3266	0.4018	0.9256	0.8203	0.7344
ROBE	Bias	-0.1370	-0.4672	-0.5652	-0.1534	-0.4916	-0.8038	-0.7811	-0.6766	-0.4955	-0.4086	-0.4134	-0.5954
	rmse	0.7193	0.5541	0.6719	0.4168	0.5750	0.8555	0.8326	0.7577	0.5927	0.5684	0.6799	0.6797

to other seasons. The maximum average monthly bias is -0.959 cm in June at station Asab, and has variations in the range of -0.959 cm (in June at station Asab) and 0.0075 cm (in June at Arba Minch. Similarly, the average monthly PW RMSE varies in the ranges of 0.2628 cm in August at Bahr Dar and 1.374 cm in March at Asab. A summary of monthly average biases and RMSEs statistics for the selected station are given in Table 6.6.

Chapter 7

Conclusion

In the modified SHAO-C model, the neutral atmospheric zenith delay is directly modeled using ERA-Interim reanalysis with high resolution 0.75×0.75 latitude by longitude grid. The performance of the model in reproducing the model zenith delay has been evaluated. The model decreasing rates and accelerating rate coefficients show seasonal variation due to different sources of moisture fields, and its correlation coefficient is in the range of 0 and 0.5 for ZTD a_1, 0.5 and 1 for ZTD a_2, -0.05 and 0.05 for ZWD a_{w1}, and -0.1 and 0.1 for ZWD a_{w2}. The mean ZTD_{mean} and ZWD_{mean} ranges from 1.8 m to 2.5 m and 0.1m to 0.22m respectively over the region. However, the mean annual amplitude variation ZTD_{amp} and ZWD_{amp} range from 0.02 m to 0.1 m over the region.

The comparision of the model zenith total delays, zenith wet delays and the derived PW with corresponding GPS measurement shows very good agreement especially in summer season. For most of the GPS stations, the average monthly bias and RMSE during 2007-2011 in ZTD , ZWD and PW are less than 6.23 cm, 4.5cm and 0.97 cm, respectively. Similarly, the mean daily bias in ZTD, ZWD and PW range from -4.3 cm to -2 cm, -3.42 cm to -0.584 cm and -1.12 cm to -0.34 cm respectively. The variability in ZTDs arises from the variability of ZWD.

However the bias and RMSE values of the model ZTD, ZWD and PW are generally higher in summer (high negative bias) than winter (small positive bias). Furthermore, RMSE decreases as the altitude increases while its variation with latitude and longitude is not very obvious over Ethiopia and its neighbor.

Therefore, the modified SHAO-C model is accurate enough and can be used to estimate ZTD for navigation and positioning purpose as real-time tropospheric delay correction at user height over Ethiopia.

Appendix A

Metrological input for GAMIT/GLOBK

A.1 sestbl.

A session control table (sestbl.) with only the required and commonly used entries for meteorological file is shown below.

```
Zenith Delay Estimation = Y ; Yes/No (default No)
Interval zen = 2 ; 2 hrs = 13 knots/day (default is 1 ZD per day)
Zenith Constraints=0.50;zenith-delay a priori constraint in meters(default0.5)
Zenith Model = PWL ; PWL (piecewise linear)/CON (step)
Zenith Constraints=0.50;zenith-delay a priori constraint meters(default 0.5)
Zenith Variation =0.02 100.  ;zenith-delay variation,tau in meters/sqrt(hr),hrs
              (default.02 100.)
```

We Specify $IntervalZen = 2$ to get estimates at 2-hr intervals for a 24 hr session, and PWL (Piecewise Linear) for Zenith Model will invoke a single parameter for the zenith delay over the session or (representation includes tabular points on each end of the observation span). The first value in Zenith Variation is the point to point variation allowed, in units of meters and the second value is the correlation time (tau)in hours. Setting *tau* long compared to the observation span results in a random walk process, which is both reasonable and easy to interpret (and has the practical advantage of persistence with large error bars for spans with few observations). The default value of 100. hrs accomplishes this for 24-hr spans.

There is an additional entry in the sestbl.,

```
Tropospheric Constraints = NO; YES/NO
```

which invokes a spatial constraint on the zenith-delay parameters. This constraint can be useful for tying together the zenith-delay adjustments for closely-spaced sites in a network.

A.2 sittbl.

Different values for the zenith constraints can be invoked using station table (sittbl.) entries, shown below:

```
SITE                FIX       --COORD.CONSTR.--
ALL                 NONE      100.  100.  100.
ADIS ADIS GPS       NONE      0.050 0.050 0.05
BHR1 BHR1 GPS       NONE      0.050 0.050 0.05
BHR2 BHR2 GPS       NONE      0.050 0.050 0.05
MAL2 MAL2 GPS       NONE      0.050 0.050 0.05
```

It is currently a requirement that the number of zenith delays in the session be the same for all stations.

A.3 Broadcast Ephemeris

The sample of navigation (broadcast ephemeris) files, with an ephemeris block for only one satellite entry, is given below:

```
     1              NAVIGATION DATA                         RINEX VERSION / TYPE
MAKEX v. 7.1 of 90/07/09 apollo   king  1990-07-06 19:16:30 PGM / RUN BY / DATE

 8 88 11  8  4  8  59.1    0.323700718582E-03     0.171894498635E-09    -0.277555756156E-16
    0.102400000000E+05     0.104687500000E+02     0.177400246575E-08    -0.199337541371E+01
    0.603497028351E-06     0.530868989881E-02     0.652857124805E-05     0.515373352242E+04
    0.194400000000E+06    -0.856816768646E-07     0.108490472307E+01     0.186264514923E-07
    0.110755363248E+01     0.330250000000E+03    -0.584334212505E+00    -0.634633577893E-08
    0.274297139863E-09     0.100000000000E+01     0.461000000000E+03     0.000000000000E+00
    0.700000000000E+01     0.600000000000E+02     0.000000000000E+00     0.102400000000E+05
```

A.4 RINEX observation file

The sample of RINEX (Receiver INdependent EXchange) files entries are shown below.

```
1.0                 COMPACT RINEX FORMAT                        CRINEX VERS   / TYPE
RNX2CRX ver.u.2.4.2                       08-Jul-08 16:57       CRINEX PROG / DATE
     2.11           OBSERVATION DATA    G (GPS)                RINEX VERSION / TYPE
teqc  2008Jul2      UNAVCO Archive Ops  20080708 16:57:02UTCPGM / RUN BY / DATE
Solaris 5.10|UltraSparc IIIi|cc -xarch=v9 SC5.8|=+|*Sparc     COMMENT
BIT 2 OF LLI FLAGS DATA COLLECTED UNDER A/S CONDITION         COMMENT
ARMI                                                          MARKER NAME
                                                              MARKER NUMBER
Reilinger, Bendick  MIT, U of Montana                         OBSERVER / AGENCY
0220310307          TRIMBLE 5700         1.24                 REC # / TYPE / VERS
12379609            TRM41249.00     NONE                      ANT # / TYPE
  5028848.3854  3867264.4030   669249.9247                    APPROX POSITION XYZ
        0.0000        0.0000        0.0000                    ANTENNA: DELTA H/E/N
     1     1                                                  WAVELENGTH FACT L1/2
     7    L1    L2    C1    P2    P1    S1    S2             # / TYPES OF OBSERV
    30.0000                                                   INTERVAL
RINEX file created by UNAVCO GPS Archive.                     COMMENT
For more information contact archive@unavco.org               COMMENT
Monument ID: 21736                                            COMMENT
UNAVCO 4-char name:   ARMI                                    COMMENT
4-char name from Log or data file: ARMI                       COMMENT
Monument location: 6.062424 37.560857 1201.8                  COMMENT
Visit ID: 93655                                               COMMENT
End of DB comments                                            COMMENT
 SNR is mapped to RINEX snr flag value [0-9]                  COMMENT
  L1 & L2: min(max(int(snr_dBHz/6), 0), 9)                    COMMENT
  2008     1     1     0     0   30.0000000     GPS           TIME OF FIRST OBS
                                                              END OF HEADER
```

A.5 Station info (station information)

An example for station info (station information) entries are given below: Where SITE

```
# Station.info written by MSTINF user root          on 2012-05-01  01:26
* Refrence file : station.info
*
*
*SITE  Station Name      Session Start      Session Stop       Ant Ht   HtCod  Ant N    Ant E    Receiver Type       Vers                 SwVer
Receiver SN          Antenna Type     Dome   Antenna SN
 ADIS  Addis Ababa Univ  2007 180  0  0  0  2008  71  7  0  0   0.0010  DHARP   0.0000   0.0000  TRIMBLE 4000SSI     7.29                 7.29
3247A01971           TRM29659.00     NONE   0220173805
 ADIS  Addis Ababa Univ  2008  71  7  0  0  9999 999  0  0  0   0.0010  DHARP   0.0000   0.0000  JPS LEGACY          2.6.1                2.60
MT30010291           TRM29659.00     NONE   0220173805
```

is the 4-character code for the observing site (monument), Station Name a 16-character description (carried for documentation only), Session Start and Session Stop the start/stop times for the entries, and Ant Ht the antenna height above the monument, HtCod indicates what physical point on the antenna structure the height refers to and whether it is a direct or slant height, and receiver type (either a 6-character GAMIT code or a 20-character RINEX-standard)and antenna (AntCod or Antenna Type) are indicate the type of receiver and receiver antenna.

Appendix B

GAMIT/GLOBK Meteorological file output

A meteorological files output of GAMIT/GLOBK are shown below. The first five columns are illustrates time (Year, day of year, hours, Minuit and second respectively). The sixth, seventh, thirteenth and eighth columns are zenith total delay (ZTD), zenith wet delay (ZWD), Zenith hydrostatics delay (ZHD) and standard division of the zenith total delay in millimeters (mm) respectively. The ninth, tenth, eleventh, and twelve-th are precipitable water vapor (PW) in millimeters (mm), standard division of precipitable water vapor in millimeters (mm), pressure in hecto-Pascal (hPa) and temperature in Kelvin (K). The last three columns (fourteenth, fifteenth, and sixteenth columns) are atmospheric delay gradient parameters, which represents atmospheric gradient of north south (NS), standard division gradient of north south and standard division gradient of east west (EW) in millimeters (mm).

```
* Estimated atmospheric values for ADIS. Height estimate:  2441.0133 +/- 0.0000 m.
* METUTIL Version 3.0  2009-08-27
* Input files: oexpta.021       zadis8.021              ZTD-file sigmas scaled by   1.0
* Yr  Doy Hr Mn Sec  Total Zen  Wet Zen  Sig Zen    PW   Sig PW (mm)  Press (hPa)  Temp (K) ZHD (mm)   Grad NS   Sig NS  Grad EW   Sig EW (mm)
 2008  21 10  0  0.    1801.60    74.80   27.10   11.90    4.31         755.90       284.90   1726.80     5.07    29.15   -46.84    32.92
 2008  21 12  0  0.    1804.50    77.70   20.80   12.36    3.31         755.90       284.90   1726.80     4.80    28.00   -47.15    31.61
 2008  21 14  0  0.    1811.80    85.00   20.40   13.52    3.24         755.90       284.90   1726.80     4.53    26.81   -47.46    30.24
 2008  21 16  0  0.    1830.70   103.90   20.30   16.52    3.23         755.90       284.90   1726.80     4.27    25.56   -47.77    28.82
 2008  21 18  0  0.    1826.90   100.10   20.50   15.92    3.26         755.90       284.90   1726.80     4.00    24.25   -48.07    27.31
 2008  21 20  0  0.    1825.40    98.60   20.40   15.68    3.24         755.90       284.90   1726.80     3.73    22.86   -48.38    25.72
 2008  21 22  0  0.    1823.90    97.10   20.40   15.44    3.24         755.90       284.90   1726.80     3.47    21.39   -48.69    24.03
 2008  22  0  0  0.    1828.00   101.20   21.00   16.10    3.34         755.90       284.90   1726.80     3.20    19.80   -49.00    22.20
```

Reference

1. Bernhard Hofmann-Wellenhof, Herbert Lichtenegger, Elmar Wasle, (2008). GNSS Global Navigation Satellite Systems GPS, GLONASS, Galileo, pp. 56-67, pp. 105-107, pp. 118, pp. 135.

2. Bevis, M., S. Businger, T.A. Herring, C. Rocken, R.A. Anthes and R.H. Ware (1992), GPS meteorology: sensing of atmospheric water vapor using the Global Positioning System, Journal of Geophysical Research, Vol. 97, No. D14, pp. 15787-15801.

3. Virgilio de Birto Mendes, Richard B. Langley, (1989), Modeling the Neutral Atmosphere propagation delay in Radiometric space techniques, pp. 1, pp. 44-62.

4. SONG ShuLi. (2011)., Establishment of a new tropospheric delay correction model over China area

5. Chen Q M, Song S L, Stefan H, et al, (2011). Assessment of ZTD derived from ECMWF/NCEP data in China. GPS Solut, doi: 10.1007/ s10291-010-0200-x

6. Gizaw Mengistu Tsidu, Yohannes Getachew and Gereab Kidanu (2012). Inter-comparison of atmospheric precipitable water from ground-based GPS measurements and ERA-Interim Reanalyis over Eastern Africa. (Chapman Longitude and Hemispheric Dependence of Space Weather conference, Addis Ababa, Ethiopia), Dept. of Physics, Addis Ababa University, Ethiopia.

7. Pratap Misra and Per Enge, (2006). Global Positioning System,signals Measurement and performance, second edition, pp. 33-36, pp. 49, pp. 79, pp. 148-171.

8. Garmin, (2008), GPS Beginner's Guide

9. Sudhir Man Shrestha, (2003), Investigations into the Estimation of Tropospheric Delay and Wet Refractivity Using GPS Measurements

10. Herring T A, King R W, McClusky S C. (2010). Document for the GAMIT GPS analysis software, release 10.4.

11. Moldwin, (2008),Institute of Geophysics and Planetary Physics University of California: An Introduction to Space Weather, pp. 72-73

12. Klo91. J.A. Klobucha, (1991). Ionospheric Effects on GPS. GPS World, 2(4):4851.

13. Saastamoinen J (1973): Contribution to the theory of atmospheric refraction. Bulletin Go- dsique, 107: 1334.

14. Griffiths D.J. (1999). In Introduction to Electrodynamics, 3rd edn.djvu, pp. 406.

15. Thayer G. (1974). An improved equation for the radio refractive index of air. radio sci... 9(10) 803-807

16. Thomas Karl Pany (2002). Development and Applications of Troposphere GPS Slant Delay Models Based on Numerical Weather Predication Models Turbalnce Theory

17. Kleijer, F. (2004) Troposphere Modeling and Filtering for Precise GPS Leveling, ISBN 90-804147-3-5, pp. 21-32

18. Battan, L.J. (1973). Rador observation of the atmosphere. University of Chicago press. pp. 324 .

19. Doviak, R.J and D.S.Zrnic, (1993). Doppler radar and weather observations. 2nd Ed. Academic press, pp. 562 . Systems, edited by D. Richter and T. Springer (Springer Verlag, Berlin, Germany, 1988), pp. 214219 .

20. Saastamioinen J (1972) Contributions to the theory atmospheric refraction, Part II Refraction corrections in satellite Geodesy. Bull Geo 105:279298

21. Hopfield HS (1969): Two-quartic tropospheric refractivity profile for correcting satellite data. Journal of Geophysical Research, 74(18): 44874499.

22. Chao, CC. (1971a). 'New tropospheric range corrections with seasonal adjustment." Jet Propulsion Laboratory, California Inst itute of Technology, Pasadena, Calif., JPL Technical RepoMisrart 32-1526, Vol. VI, pp. 67-82.

23. Chao, CC. (1973). "A new method to predict wet zenith range correction from surface measurements." In: The Deep Space Network Progress Report, Jet Propulsion Lab,Every day the ECMWF makes a forecast up to ten days a head Pasadena, Calif., JPL Technical Report 32-1526, Vol. XIV, pp. 33-41.

24. Ifadis, I.M. (1986), The atmospheric delay of radio waves: modeling the elevation dependence on a global scale, School of Electrical and Computer Engineering, Chalmers University of Technology, Goteborg, Sweden, Technical Report No. 38L, pp. 115.

25. Berman, A.L. (1976), The prediction of zenith range refraction from surface measurements of meteorological parameters, Jet Propulsion Laboratory, California Institute of Technology, Pasadena, Calif., National Aeronautics and Space Administration Technical Report 32-1602, pp. 40.

26. Rodrigo Leandro, Marcelo Santos, and Richard B. Langley (2004). UNB Neutral Atmosphere Models: Development and Performance

27. ECMWF, (1995). user Guide to ECMWF products. Metrological Bulletin M3.2, ECMWF, reading , UK.

28. Zhang J, Lachapelle G. (2001). Precise estimation of residual tropospheric delays using a regional GPS network for RTK applications. Journal of Geodesy 75: 255-266.

Declaration

This thesis is my original work, has not been presented for a degree in any other University and that all the sources of material used for the thesis have been dully acknowledged.

Name: Yohannes Getachew
Signature:– – – – – – – – – – – –

Place and time of submission: Addis Ababa University, June 2013

This thesis has been submitted for examination with my approval as University advisor.
Name: Dr. Gizaw Mengistu

Signature:– – – – – – – – – ––